

The Value of the High, Low and Close in the Estimation of Brownian Motion: Extended Version

Kurt Riedel*

Abstract

The conditional density of Brownian motion is considered given the max, $B(t|\max)$, as well as those with additional information: $B(t|\text{close}, \max)$, $B(t|\text{close}, \max, \min)$ and $B(t|\max, \min)$ where the close is the final value: $B(t=1) = c$ and $t \in [0, 1]$. The conditional expectation and conditional variance of Brownian motion are evaluated subject to one or more of the the close (final value), the high (maximum), the low (minimum). Computational results displaying both the expectation and variance in time are presented and compared with the theoretical values. We tabulate the time averaged variance of Brownian motion conditional on knowing various extremal properties of the motion. The final table shows that knowing the high is more useful than knowing the final value among other results. Knowing the open, high, low and close reduces the time averaged variance to 42% of the value of knowing only the open and close (Brownian bridge).

Keywords: Brownian motion, Brownian maximum, Brownian paths.

AMS MSC 2010: 60J65, 60J70, 91G60.

Submitted to on Aug14, 2019, final version accepted on FIXME!.

May 16, 2022

1 Introduction

Classically, most of the financial forecasting based on charts uses at most four pieces of information for each day, the opening price (open), the closing price (close), the maximum price (high) and the minimum price, (low) [18]. We address the issue of how much additional information the high and low carry beyond that of the open and close. We measure the "value" by the reduction of the variance of the Brownian motion given one or both of the high and low.

In today's financial markets, every tick is archived. In analyzing events in the ancient past (1970s) or less automated markets like credit default swaps or emerging market bonds (roughly pre-2013), the only data that typically is available is open, high, low, close data. An entire field, chartist analysis, uses these descriptors as the "sufficient statistics" for prediction. This paper defines the probability distribution of $B(t|\text{high}, \text{low}, \text{close})$ and calculates its expectation. Our formulas allow us to interpolate the price signal as $E[B(t|\text{open}, \text{high}, \text{low}, \text{close})]$ over all time in $[0, 1]$ given any data source that only has open, high, low, close data.

There have been a number of studies that use the open, high, low and close to improve the estimate of the volatility (standard deviation) of the Brownian motion [11, 16, 17, 20]. In contrast, we assume that the variance is given and standardized to one. In reality, the volatility of financial time series are unknown, bursty, and temporally non-uniform on many time scales. Given a model of the time dependence of the volatility, one must transform time to an equal volatility time. For this paper, we neglect this difficult problem and proceed with the studying standardized Brownian motion.

Let $B(t)$ be the standard Brownian motion on $[0, 1]$ and $B_c(t)$ be the Brownian motion restricted to $B_c(t=1) = c$. Our notation tracks the excellent compendium of results by Devroye [6]. Many of the results summarized in Sections 2 can be found there. The variance of the path of a Brownian motion is $V(t) = t$ which integrates to $\int_0^1 V(s) = 1/2$. For the Brownian bridge pinned to $B(t) = c$, the variance is independent of the terminal value, c , and satisfies $V(t) = t(1-t)$.

*Millennium Partners LLC E-mail: kurt.riedel@gmail.com

Integrating variance of the Brownian bridge from zero to one yields an average variance, $\int_0^1 V(s) = 1/6$. Thus knowledge of both the open and the close significantly reduces the variance of the process. Now suppose that we know the value of restricted Brownian motion at a point t_o with $0 < t_o < 1$. The variance of this pinned process satisfies $V(t) = t(1 - t/t_o)$ for $0 \leq t \leq t_o$ and $V(t) = t - t_o$ for $t > t_o$. Integrating the pinned $V(t)$ yields $\int_0^1 V(s) = t_o^2/6 + (1 - t_o)^2/2$. This variance is minimized at $t_o = .75$ with an average variance of .125. This shows that one minimizes the uncertainty during the day by recording not the final value of the Brownian motion but the value at $time = .75$. The 25% reduction in the variance by shifting the time point to $t_o = .75$ is much smaller than the increase in variance for $t_o < .5$. For finance, we are often interested in forecasting the overnight return. In these cases, the closing value may be more valuable than having the value at time equal .75.

We consider the distribution of $B(t)$ conditioned on one or more of $B(t = 1) = c$, $\max_{t \in [0,1]} B(t) = h$ and $\min_{t \in [0,1]} B(t) = \ell$. We evaluate the conditional density of $B(t|close, max)$ and $B(t|close, max, min)$ using Chapman-Kolmogorov type calculations. The conditional densities of $B(t|max)$ and $B(t|max, min)$ are found by integrating the earlier densities over c . Our primary goal is to evaluate the conditional mean and conditional variance of $B(t)$ in these cases. For several cases, explicit formulas for the moments are given. The location of the minimum and the location of the maximum are unknown in our analysis.

Section 2 reviews results on the density/distribution of extrema of Brownian motion. Section 3 derives analytic formulæ for $E[B(t|c, h)]$ and $Var[B(t|c, h)]$. Section 4 reviews our numerical simulations. Section 5 plots $E[B(t|c)]$ and $Var[B(t|c)]$ as well as $E[B(t|h)]$ and $Var[B(t|h)]$. It then computes Feller's distribution for the range, $\Delta = h - \ell$, and compares with our simulation results. Section 6 plots the $E[B(t|c, h)]$ and $Var[B(t|c, h)]$ for a variety of different values of (c, h) . Section 7 compares the analytic formulæ in Section 3 with the simulation results in Section 6. Section 8 derives analytic formulæ for $E[B(t|c, h, \ell)]$ and $Var[B(t|c, h, \ell)]$. Section 9 plots the $E[B(t|c, h, \ell)]$ and $Var[B(t|c, h, \ell)]$ for a variety of different values of (c, h, ℓ) . Section 10 compares the analytic formulæ in Section 8 with the simulation results in Section 9. Section 12 discusses and summarizes results. Especially important are Table 1 and Figure 31.

2 Distributions of Brownian Extrema

The study of Brownian extrema date back to the founders of the field [15]. Our brief discussion follows [6] with additional results taken from [21], [8], [7] and [13]. We denote the Gaussian density by $\phi_s(x) = (2\pi s)^{-0.5} \exp(-x^2/2s)$. The density of the high, (maximum of $B(t)$), h is that of the half normal: $2|\phi_1(h)| = p(h) = \sqrt{\frac{2}{\pi}} \exp(-h^2/2)$, $h > 0$. In [21, 14], the joint distribution of the close, c , the high, h , and the location of the high, θ , is shown to be:

$$p(\theta, h, c) = \frac{h(h - c)}{\pi\theta^{3/2}(1 - \theta)^{3/2}} \exp\left(-\frac{h^2}{2\theta} - \frac{(h - c)^2}{2(1 - \theta)}\right), \quad h \geq 0, h \geq c. \tag{2.1}$$

The marginal density of the maximum, h , and $c = B(1)$ is obtained by integrating (2.1) over θ :

$$p(h, c) = P(h = \max\{B(s), s \in [0, 1]\}, B(1) = c) = \frac{2(2h - c) \exp(-(2h - c)^2/2)}{\sqrt{2\pi}}, \tag{2.2}$$

where $h \geq 0, h \geq c$. [22, 12]. The conditional density, $p(c|h)$, is given by

$$p(c|h) = p(h, c)/p(h) = \frac{(2h - c) \exp(-(2h - c)^2/2)}{\exp(-h^2/2)}. \tag{2.3}$$

The distribution of the high, given the closing value, $B(1) = c$, is

$$F(h|c) = 1 - \exp(-(c^2 - (2h - c)^2)/2). \tag{2.4}$$

The density for (2.4) can be computed using [16, 6]:

$$H_c \equiv \max B(t|B(1) = c) \stackrel{L}{\sim} c/2 + \sqrt{c^2 + 2\chi}/2, \tag{2.5}$$

where χ is an exponentially distributed random variable. Using (2.3), we find

$$E[c|h] = h - \sqrt{\frac{\pi}{2}} \operatorname{erfc}\left(\frac{h}{\sqrt{2}}\right) \exp(h^2/2), \quad E[c^2|h] = h^2 + 2 - 4h\sqrt{\frac{\pi}{2}} \operatorname{erfc}\left(\frac{h}{\sqrt{2}}\right) \exp(h^2/2), \quad (2.6)$$

$$\operatorname{Var}[c|h] = h^2 + 2 - 2h\sqrt{\frac{\pi}{2}} \operatorname{erfc}\left(\frac{h}{\sqrt{2}}\right) \exp(h^2/2) - \frac{\pi}{2} \left[\operatorname{erfc}\left(\frac{h}{\sqrt{2}}\right) \exp(h^2/2) \right]^2. \quad (2.7)$$

Similarly, $m_c \equiv \min B(t|B(1) = c) \stackrel{L}{\sim} c/2 - \sqrt{c^2 + 2\chi}/2$.

A result that goes back to Levy [15, 5], if not earlier, is

$$P(B(t = 1) = c, \ell \leq B(t) \leq h) = \sum_{k=-\infty}^{\infty} \phi(c - 2k(h - \ell)) - \phi(c - 2h - 2k(h - \ell)) \quad (2.8)$$

$$= \phi(c) - \sum_{k=0}^{\infty} [\phi(c - 2h - 2k\Delta) + \phi(c - 2\ell + 2k\Delta)] + \sum_{k=1}^{\infty} [\phi(c - 2k\Delta) + \phi(c + 2k\Delta)] \quad (2.9)$$

where $\Delta \equiv (h - \ell)$. The symmetric form, (2.9), not only treats h and ℓ symmetrically, but also shows the series is in an alternating form. There is a third form of (2.8) that replaces $\phi(c - 2h - 2k\Delta)$ with $\phi(c - 2\ell + 2k\Delta)$. This form shows that $P(B(t = 1) = h, \ell \leq B(t) \leq h) = 0$.

To calculate the density, we use $p(h, \ell, c) = -\partial_\ell \partial_h P(B(t = 1) = c, \ell \leq B(t) \leq h)$.

$$p(h, \ell, c) = 4 \sum_{k=-\infty}^{\infty} k^2 a_k(c, \Delta) \phi(c - 2k\Delta) - k(k + 1) a_k(c - 2h, \Delta) \phi(c - 2h - 2k\Delta), \quad (2.10)$$

where $a_k(c, \Delta) \equiv (c - 2k\Delta)^2 - 1$. To evaluate the density, $p(h, \ell)$, we integrate $p(h, \ell, c)$ from L to H and then set $L = \ell$ and $H = h$:

$$p(h, \ell) = -\partial_\ell \partial_h \int_L^H P(B(t = 1) = c, \ell \leq B(t) \leq h) dc = \quad (2.11)$$

$$-4 \sum_{k=-\infty}^{\infty} k^2 [h_k \phi(h_k) - \ell_k \phi(\ell_k)] - k(k + 1) [(h_k - 2h) \phi(h_k - 2h) - (\ell_k - 2h) \phi(\ell_k - 2h)], \quad (2.12)$$

where $h_k \equiv h - 2k\Delta$ and $\ell_k \equiv \ell - 2k\Delta$.

3 Density Given High and Close

We derive the density, $P(B(t) = x|B(1) = c, \max\{B(s)\} = h)$ and then compute the first and second moments. Clearly,

$$P(B(t) = x|B(1) = c, \max\{B(s)\} = h) = P(B(t) = x, B(1) = c, \max\{B(s)\} = h) / p(h, c). \quad (3.1)$$

The divisor, $p(h, c)$, is the well-known probability and given by (2.2). We decompose $P(B(t) = x, B(1) = c, \max\{B(s)\} = h)$:

$$P(B(t) = x, B(1) = c, \max\{B(s)\} = h) = P_{t,x}(h) Q_{1-t,c-x}(h - x) + Q_{t,x}(h) P_{1-t,c-x}(h - x). \quad (3.2)$$

Here

$$P_{t,x}(h) \equiv P(\max\{B_x(s), s \in [0, t]\} \leq h) = \phi_t(x) - \phi_t(2h - x) \quad (3.3)$$

$$Q_{t,x}(h) \equiv P(\max\{B_x(s), s \in [0, t]\} = h) = \frac{dP_{t,x}(h)}{dh} = \frac{2(2h - x)}{t} \phi_t(2h - x) \quad (3.4)$$

$$P_{1-t,c-x}(h - x) \equiv P(\max\{B_{c-x}(s), s \in [t, 1]\} \leq h - x) = \phi_{1-t}(c - x) - \phi_{1-t}(2h - c - x) \quad (3.5)$$

$$Q_{1-t,c-x}(h-x) \equiv P(\max\{B_{c-x}(s), s \in [t, 1]\} = h-x) = \frac{2(2h-c-x)}{1-t} \phi_{1-t}(2h-c-x). \quad (3.6)$$

Equation (3.2) simply states that if the realization goes through the points (t, x) and $(1, c)$ and has a high value of h , then either it reaches h in $[0, t]$ or in $[t, 1]$. Equation (3.2) is the kernel of the Chapman-Kolmogorov representation for this restricted Brownian motion problem. We define the function

$$F(x, t, h, c) \equiv P(B(t) = x, B(t) \leq h) \times P(B(1-t) = c-x, B(1-t) \leq h-x). \quad (3.7)$$

The sum of the terms in the square brackets of (3.2) is just $\frac{\partial F}{\partial h}(x, t, c, h)$. Note that $F(x, t, h, c)$ is the difference of four Gaussian. We write (3.7) as

$$F(x, t, h, c) = \frac{1}{2\pi\sigma(t)} [f_1(x, t, c) - f_2(x, t, c, h) - f_3(x, t, c, h) + f_4(x, t, c, h)], \quad (3.8)$$

where $\sigma^2(t) \equiv t(1-t)$. All four terms, f_i , are of the form:

$$f_i(x, t, h, c) = \exp\left(-\frac{(1-t)(x-a_i)^2 + (x-b_i)^2 t}{2t(1-t)}\right) = \exp\left(-\frac{(x-\mu_i(t, c, h))^2}{2\sigma^2}\right) \exp^{-g_i(c, h)} \quad (3.9)$$

where $a_1 = 0, b_1 = c, a_2 = 0, b_2 = 2h-c, a_3 = 2h, b_3 = c, a_4 = 2h, b_4 = 2h-c$. Here we define

$$\mu_i(t, c, h) \equiv a_i(1-t) + b_i t; \quad g_i \equiv \frac{[a_i^2(1-t) + b_i^2 t] - \mu_i^2}{2\sigma^2} = (a_i - b_i)^2 / 2. \quad (3.10)$$

Thus, $\mu_1 = ct, g_1 = c^2/2, \mu_2 = (2h-c)t, g_2 = (2h-c)^2/2, \mu_3 = 2h(1-t) + ct, g_3 = (2h-c)^2/2$ and $\mu_4 = 2h-ct, g_4 = c^2/2$. It is often convenient to define $r = r(h, c) = 2h-c$. Using $r, \mu_2 = rt, g_2 = r^2/2, \mu_3 = 2h-rt, g_3 = r^2/2$. Note that $f_i(x = h, t, h, c) = 2\pi\sigma\phi_t(h)\phi_{1-t}(h-c)$. The equality of the four terms at $x = h$ will allow us to cancel terms when we integrate by parts. To simplify our calculations, observe

$$\partial_h f_i = \left[\frac{(x-\mu_i)}{\sigma^2} \partial_h \mu_i - \partial_h g_i \right] f_i \quad \text{and} \quad \partial_x f_i = -\frac{(x-\mu_i)}{\sigma^2} f_i. \quad (3.11)$$

Note f_1 is independent of h and therefore may be ignored. Derivatives of $F(x, t, h, c)$ with respect to h only enter through h dependencies in μ_i and g_i . Let $s_i = -1$ for $i = 2, 3$ and $s_i = 1$ for $i = 1, 4$. We define $\tau_i \equiv .5 * \partial_h \mu_i$ so that $\tau_2 = t, \tau_3 = 1-t, \tau_4 = 1$. Checking the normalization:

$$\int_{-\infty}^H \partial_h F(x, t, h, c) dx = \frac{1}{2\pi\sigma} \sum_{i=2}^4 \int_{-\infty}^H s_i \partial_h f_i(x, t, h, c) dx = \quad (3.12)$$

$$\frac{-1}{2\pi\sigma} \int_{-\infty}^H \left[\sum_{i=2}^4 s_i \partial_h \mu_i \partial_x f_i + 2(2h-c)(f_2 + f_3) \right] dx = \quad (3.13)$$

$$\frac{1}{\pi\sigma} \left[-\sum_{i=2}^4 s_i \tau_i f_i(x = h) \right] + \frac{2h-c}{\pi\sigma} \int_{-\infty}^H (f_2 + f_3) dx = p(h, c). \quad (3.14)$$

We use H to denote the upper limit which is evaluated at $H = h$. The point of using a different symbol is that when we differentiate with respect to h , the upper limit H is not differentiated. Now we compute the moments

$$M_m(h, c) = \int_{-\infty}^H x^m \partial_h F(x, t, h, c) dx = \sum_{i=2}^4 \frac{s_i}{2\pi\sigma} \int_{-\infty}^H x^m \left[-\partial_h \mu_i \partial_x f_i - \frac{\partial_h g_i}{2} \right] f_i = \quad (3.15)$$

$$\sum_{i=2}^4 \frac{s_i}{2\pi\sigma} \int_{-\infty}^H [m x^{m-1} \partial_h \mu_i - \partial_h g_i x^m] f_i dx = \quad (3.16)$$

$$\sum_{i=2}^4 \frac{2s_i}{\sqrt{2\pi}} e^{-\frac{g_i}{2}} \int_{-\infty}^{H-\mu_i} [m(x+\mu_i)^{m-1} \tau_i - (2h-c)(x+\mu_i)^m (1-\delta_{i,4})] \phi_{\sigma^2}(x) dx. \quad (3.17)$$

To go from (3.15) to (3.16), we use that the three terms evaluated at $x = h$ again cancel. We evaluate $M_1(t, h, c)$ and $M_2(t, h, c)$ in the Appendix and present the results here:

$$M_1 \equiv \frac{e^{-\frac{c^2}{2}}}{\sqrt{2\pi}} [1 + \operatorname{erf}(\frac{ct-h}{\sqrt{2\sigma}})] + \frac{e^{-\frac{r^2}{2}}}{\sqrt{2\pi}} [2hr - 1 + p_{h,r,t} \operatorname{erf}(\frac{h-rt}{\sqrt{2\sigma}})] - \frac{2\sigma r}{\pi} e^{-\frac{r^2}{2}} e^{-\frac{(h-rt)^2}{2\sigma^2}} \quad (3.18)$$

where $r \equiv 2h - c$ and $p_{h,r,t} \equiv 1 - 2hr + 2t(r^2 - 1)$. The final result is $E[B(t|h, c)] = M_1(t, h, c)/p(h, c)$. The second moment is given by $E[B^2(t|h, c)] = M_2(t, h, c)/p(h, c)$ where

$$M_2 = \sqrt{\frac{2}{\pi}} (2h - ct) e^{-\frac{c^2}{2}} [1 + \operatorname{erf}(\frac{ct-h}{\sqrt{2\sigma}})] + \quad (3.19)$$

$$\sqrt{\frac{2r}{\pi}} \exp^{-\frac{r^2}{2}} \left(\left[\sigma^2 + q_1(h, c, t) + q_2(h, c, t) \frac{4h(rt-h)}{2} \operatorname{erf}(\frac{h-rt}{\sqrt{2\sigma}}) \right] - 4h\sigma^2 \phi_{\sigma}(h-rt) \right) \quad (3.20)$$

where $q_1(h, c, t) \equiv r^2 t^2 + 2h^2 - 2hrt - rt^2 - (1-t)(2h-rt)$, $q_2(h, c, t) \equiv \frac{4h(rt-h)}{2} - rt + 2h(1-t)$.

4 Numerical Methods

Simply put, we generate a large number of Brownian paths, bin the paths in (*close*, *max*, *min*) space and calculate the mean and variance for each time and bin. We order the coordinates of phase space, (q_1, q_2, q_3) , so that $q_1 = B(1)$, $q_2 = \max_{0 \leq t \leq 1} B(t)$ and $q_3 = \min_{0 \leq t \leq 1} B(t)$. We also consider the case where we replace one or more of these operators with *argmax* or *argmin*. The results for the *argmax* case are found in [19].

A very straightforward algorithm is

1) Specify a timestep, dt , a number of bins in each direction n_{bins} , and a number of sample paths, N_{samp} with typically $N_{samp} \approx \kappa n_{bins}^3$ where κ denotes the typical number of simulations in a bin. More generally, for any choice of grids for the bins, we want at least κ simulations in each bin where κ is a large number. Generate a large array of scaled Gaussian random variables, size $(N_{samp}, 1/dt)$. Cumsum them to generate an array of Brownian paths. We often use a nonuniform time step where the time step is smaller near $t = 0$ and near $t = 1$.

2) In the first phase space direction, compute bin boundaries so that the number of curves are roughly equal in each bin. For each one dimensional bin, compute bin boundaries in the second coordinate direction so that the number of bins is roughly equal. Finally, for each of the two dimensional bins, compute bins in the third direction.

3) For each of the n_{bin}^3 bins, assign a triple index, (i, j, k) bins, compute the mean of the coordinates, $(\bar{q}_1, \bar{q}_2, \bar{q}_3)$, and compute the mean, $\mu(t; \bar{q}_1, \bar{q}_2, \bar{q}_3)$, and variance, $V(t; \bar{q}_1, \bar{q}_2, \bar{q}_3)$, of $\{B(t)\}$ in the bin.

4) Test for convergence of $\mu(t; \bar{q}_1, \bar{q}_2, \bar{q}_3)$ and $V(t; \bar{q}_1, \bar{q}_2, \bar{q}_3)$ in N_{samp} , n_{bins} , and dt . This involves interpolation as grids boundaries are random functions of the particular ensemble of paths. Note that the grid boundaries for the first coordinate direction are independent of the second two coordinate directions but that the average value of q_1 will depend on all three indices, (i, j, k) . We find that interpolation from one grid to another grid broadens the width of the peaked functions especially when *argmax* is one of the given variables.

There is a bias versus variance tradeoff. If the bins are too large, the variation of the mean and variance will be obscured. If the bins are too small, there will be too few curves in each bin and the sample variance will dominate. Each of the close, max and min have a Gaussian or half Gaussian distribution individually so the tails of the distribution will be spread out. The situation is actually somewhat better as the high and low are exponentially distributed given the closing value. Nevertheless, exponential distributions have very few points in the tail of the distribution. Again, a low density of curves will significantly inflate the size of the tail bins and thereby add larger bias to the the computation

of the bin variance. Thus convergence of the mean and variance on the outermost bins is tenuous. When we compute population average variance, we are tempted to downweight or even exclude the outer bins. While this is probably a smart thing to do, we report the simple ensemble average instead of a more complex limit reducing the underweighting as the bin size goes to zero.

Assume that we wish to generate bins in the \bar{q} direction. We sort the Brownian realization in the \bar{q}_1 direction. To generate the grid boundaries, we initially tried equi-spaced quantile bins. This results in very large bins in the low density region. These large bins result in bias to our estimates for both the expectation and variance estimates. Let the density of points/curves be $n(\bar{q})$. To reduce the size of the largest bins, we select bin boundaries to keep $\int_{\bar{q}_k}^{\bar{q}_{k+1}} n(\bar{q})^\alpha d\bar{q}$ to be approximately equal where $\{\bar{q}_k\}$ are the bin boundaries. We use $\alpha = .7 - .75$ while $\alpha = 1$ corresponds to equal quantiles. We find that first and last bins converge much very slowly in $(nSim, nbin)$ space especially using a quantile based gridding. Using equal bins of $n(\bar{q})^\alpha$ partially but not completely alleviates this problem.

Wiener's Fourier representation of Brownian paths on $[0, 1]$ is

$$B(t) = \xi_0 t + \sum_{n=1}^{\infty} \xi_n \frac{\sin(nt)}{\pi n}, \quad \text{where } \{\xi_k\} \text{ are independent normal.} \tag{4.1}$$

Given an ensemble of Brownian paths, $\{B_i(t)\}$, we can create an equivalent ensemble of Brownian paths, $\{B_i(t, c)\}$, with right endpoint c , using the formula: $B_i(t, c) \equiv B_i(t) - (B_i(t = 1) - c)t$. This allows us to take one set of Brownian paths and use them on a grid of final values. This significantly reduces the number of realizations we need to cover phase space. Thus if the closing value is the first parameter direction that we examine, a 3-dimensional parameterization is reduced to a sequence of two-dimensional parameterizations.

5 Single Conditional Value

5.1 Brownian Bridge

We begin with plots of our simulation for the Brownian bridge case, i.e. Brownian motion constrained to a given closing value. For this simulation, we use 15 million simulations with $nsteps=1500$. For a given value of $B(1) = c$, the simulation yields a straight line in time for $E[B(t)|B(1) = c]$. Figure 1 plots the time dependent variance, $Var[B(t)|B(1) = c]$ for a variety of c . The closing values are chosen to be the values in bins number, $(0, 2, \dots, nbin - 3, nbin - 1)$ where the third through eighth bin are equi-spaced in bin number. The theoretical value is $t(1 - t)$ and is displayed as the red curve in Figure 1. All but the first and last curve match the theoretical values. This occurs because the first and last bins cover a very large range of c . We are averaging different values of $E[B(t)|B(1) = Close]$ and the squared bias is counted as variance.

5.2 Given High

To calculate the probability, $p(x, t, h)$, we integrate $p(x, t, h, c)$ from (3.2)-(3.6), $p(x, t, h) = \int_{-\infty}^H p(x, t, h, c) dc$. The result is

$$p(x, t, h) = 2[\phi_t(x) - \phi_t(2h - x)]\phi_{1-t}(h - x) + \frac{2(2h - x)}{t} \phi_t(2h - x) erf\left(\frac{h - x}{\sqrt{2(1 - t)}}\right) \tag{5.1}$$

The theoretical values of $E[B(t)|h]$ and $Var[B(t)|h]$ can be calculated by computing moments with respect to (5.1) and then dividing by $p(h) = 2 * \phi(t)$, $h \geq 0$.

Unfortunately, we have not found a tractable analytic form from the integrals and therefore we compute them numerically [9].

Figure 2 plots the expectation of $B(t)$ for ten values of the high. Not surprisingly, if the high occurs near $t = 0$, the expectation decreases monotonically and decreases faster for smaller t . Let $f(t, h) \equiv E[B(t)|\max B = h]$. It appears that f is smooth in t and $|\frac{\partial f}{\partial t}|$ is decreasing in time. For large values of h , $f(t, h)$ grows approximately linearly. We see that the zero of $f(t = 1, h)$ occurs somewhere

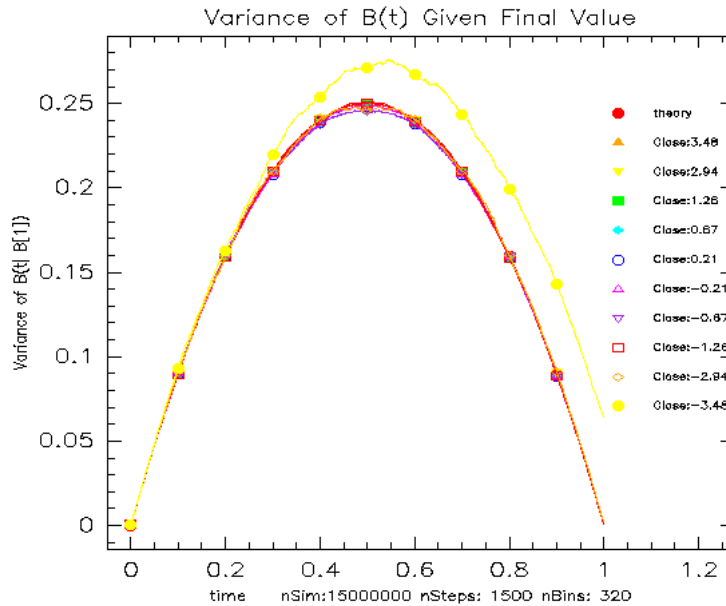


Figure 1: $Var[B(t|c)]$ for various final values, c

between $.68 < h < .95$. Using (2.6), we see the precise value is $.7517915247$. Figure 3 plots the variance of a bin as a function of time. Again, the computed variance includes the squared bias from effectively assuming that expectation is constant in each bin. Since $f(t, h)$ varies from the smallest value of h in the bin to the largest value of h in the bin, we are systematically overestimating the variance. For this particular computation, we define $vrAvg$ to be the time and ensemble average of the variance. Looking at the dependence as a function of $nbins$, the number of bins, we find $vrAvg(nbins = 80) = 0.16033$, $vrAvg(nbins = 160) = 0.16021$, $vrAvg(nbins = 320) = 0.16018$ and $vrAvg(nbins = 480) = 0.16017$. Knowing the value of the high is slightly better at reducing the time averaged variance since $vrAvg < 1/6$.

Returning to Figure 3, we see that that $var(t, h) \equiv Var[B(t)|\max B = h]$ is monotonically increasing for small values of h , up to at least $h = .67$. For larger values of h , the variance is non-monotone. This non-monotonicity occurs because at large values of h , the maximum of $B(t)$ is likely to be near $t = 1$.

Figure 2 plots the time averaged value of $f(t, h)$ versus h . The curve looks concave, smooth and possibly nearly linear for larger values of h . Figure 5 plots the square root of the time average of $Var[B(t|h)]$. Even after time averaging, the curve is noisy in its h dependence. We note that the increase in $\int_0^1 var(t, h)dt$ may contain substantial bias for the largest point(s) in h . In these simulations, we use an ensemble of 36,000,000 realizations computed with 1530 steps and bin the results into 100 bins.

For each of the ten values of the high, we display both the simulation curve and the analytic curve from numerically computing the moments of (5.1). The simulated curves have the symbols overstruck on them. The point is the match of simulation with (5.1) is very good.

5.3 Feller Range

To look at convergence, we examine the distribution of the range as a function of the number of steps in the Brownian motion simulation. The theoretical distribution was calculated by Feller in [10]: The range $R_t \equiv \max_{0 \leq s \leq t} B(s) - \min_{0 \leq s \leq t} B(s)$ at time t is distributed like $\sqrt{t}R_1$ and the density of R_1 is the function f defined on $(0, \infty)$ by $f(x) = 8 \sum_{k=1}^{\infty} (1)^{k+1} k^2 \phi(kx)$, where ϕ denotes the standard normal density [10]. As noted by Feller: "In this form it is not even obvious that the function is positive".

High, Low and Close in Brownian Estimation

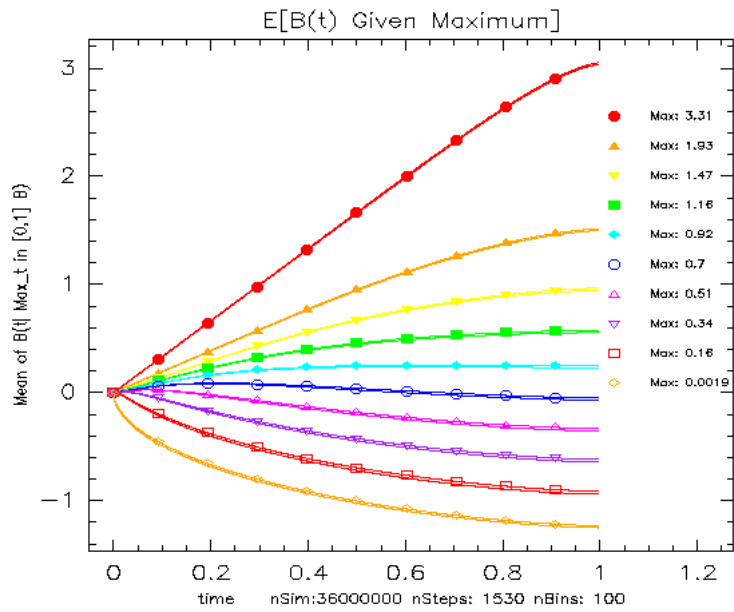


Figure 2: Expectation of $B(t)$ given $\max\{B(s)\} = h$ for various values of the high, h .

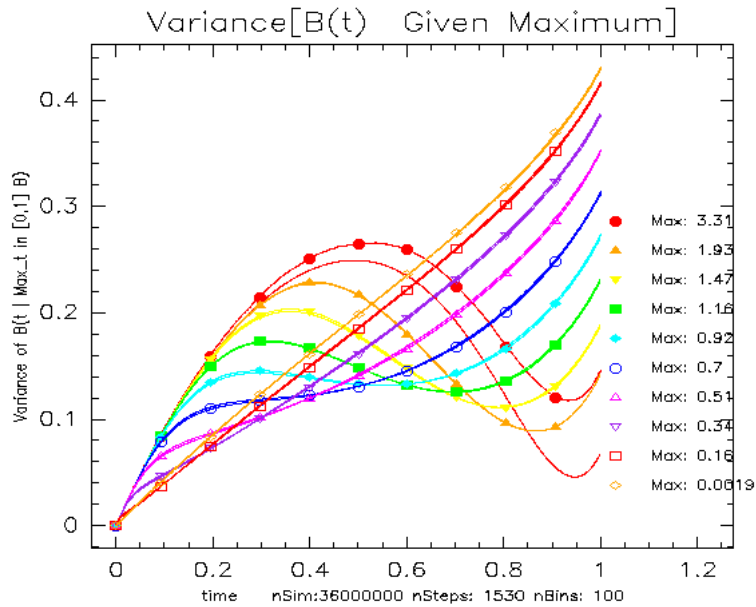


Figure 3: Variance of $B(t)$ given $\max\{B(s)\} = h$ for various values of the high, h .

High, Low and Close in Brownian Estimation

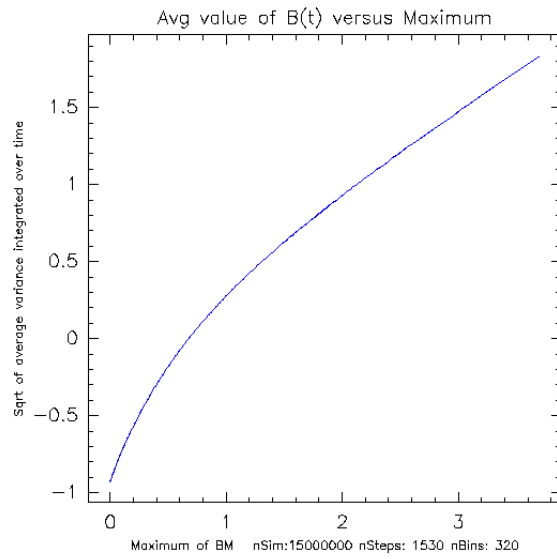


Figure 4: Time average of $E[B(t)|h]$ versus its maximum, h

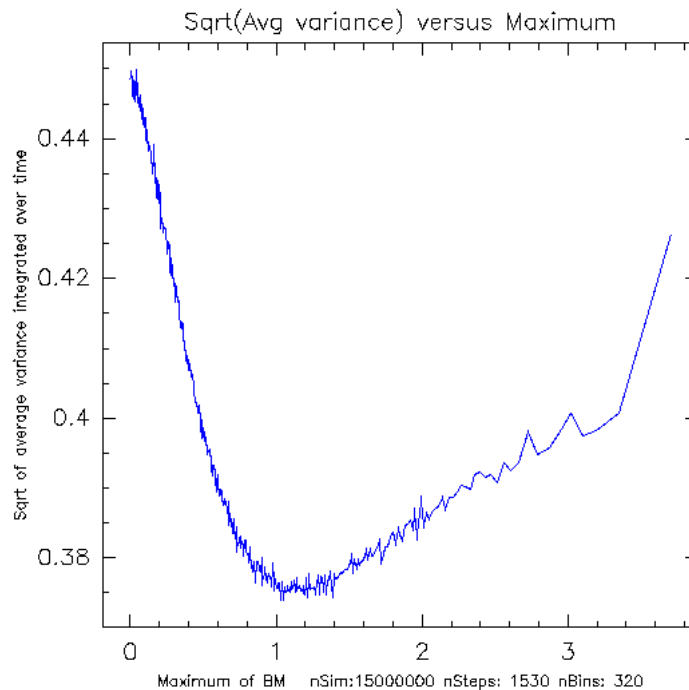


Figure 5: Square root of time average of $Var[B(t)|h]$ versus the high, h . We strongly suspect that the final point on the curve is incorrect, caused by the the squared excess bias in the final bin.

We compute Feller's formula for the density of the range of a Brownian motion. It converges very slowly near zero. To evaluate $f(x = .005)$, we need between 300 and 400 terms. The formula is useful to compare our Brownian motion computations with the theoretical results. Figure 6 compares the empirical density with Feller's result. The blue curve is computed from Feller's expansion, the black curve is the empirical density from four million realizations with 2000 time steps. The green curve uses only 500 time steps. We see very good agreement. The main difference is that the empirical distribution is shifted slightly to the left. There is less than 0.1% of the distribution below $range < 0.7$. In Section 8, the density given high and low bounds involves an expansion in $\sum_k \exp(-k^2(h-l)^2)$. This expansion converges very quickly for vast majority of the ensemble of Brownian paths.

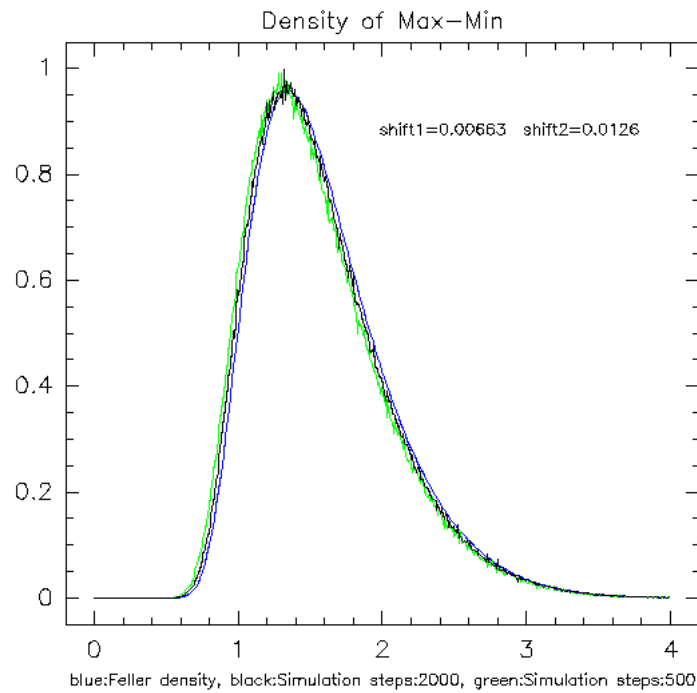


Figure 6: Density of the Range: $\max_{0 \leq s \leq 1} B(s) - \min_{0 \leq s \leq 1} B(s)$. Computation of Feller's formula uses 400 terms. Empirical distribution uses 4,000,000 simulations with 500 and 2000 time steps.

We see that the shift of the empirical distribution decreases as the step size decreases. For a step size of .0005, the shift of the center of mass of the distribution is .0066 from the theoretical result. Using a timestep four times larger doubles the shift.

The distribution of the range is very small for $range < .5$ and this region is poorly approximated by the Feller expansion. This is the clear opportunity for an asymptotic expansion in the region of small range.

6 Figures Conditional on Close, High

In this section, we plot the $E[B(t|c, h)]$ and $Var[B(t|c, h)]$ for a variety of different values of (c, h) . Specifically, we choose quantiles (.2, .5, .8) of the bin values for the close. For our robustified grid, this corresponds to $close = -1.011, 0.0152, 1.055$. In each plot, we plot the expectation $E[B(t|c, h)]$ for ten values of h . The ten values of h are chosen to be equi-spaced in the bin coordinate from the second bin to the second to the last bin. We then repeat for $Var[B(t|c, h)]$. We conclude with plots for the time average of $E[B(t|c, h)]$ and $Var[B(t|c, h)]$.

For these plots, we use 1530 time steps on each simulation for a total of 18 million simulations with 100 bins in each parameter direction. The curves overstruck by symbols are the simulation curves. The analytic formula curves have the same color but no symbol.

6.1 Time Dependent Mean Given Close, High

Figure 7 shows that the expectation is nearly monotonically decreasing for strongly negative values of the close and near zero values of the high. We say nearly decreasing because we have not examined the behavior near $time = 0$. For large value of the high, the high peaks near the middle of the time interval. Figure 8 shows the expectation is nearly symmetric in time when the close is near zero.

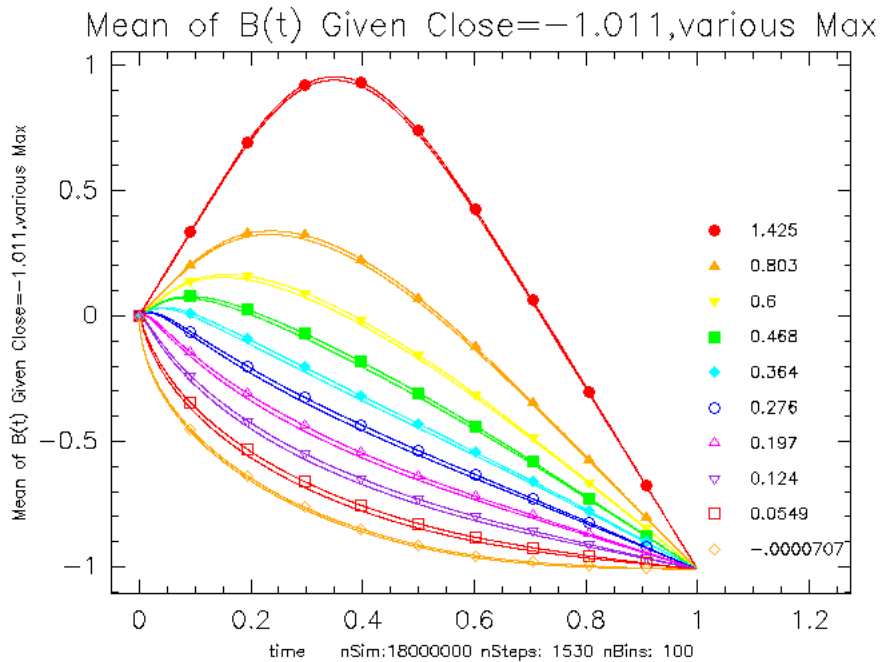


Figure 7: $E[B(t|close = -1.011, various high)]$ where the values of the maximum are given in the legend

Figure 7 and Figure 9 display the following reflection symmetry: $E[B(t - c, h)] = E[B(1 - t|c, h + c)] - c$ where $c > 0$.

6.2 Time Dependent Variance Given Close, High

Figures 10-12 display $Var[B(t|close, high)]$ for $close = -1.011, 0.0152, 1.055$. The smooth curves with no symbol are the analytic results from (3.18) and (3.19). In many cases, the variance is multimodal in time. Figure 10 and Figure 12 display the following reflection symmetry: $Var[B(t - c, h)] = Var[B(1 - t|c, h + c)]$ where $c > 0$.

High, Low and Close in Brownian Estimation

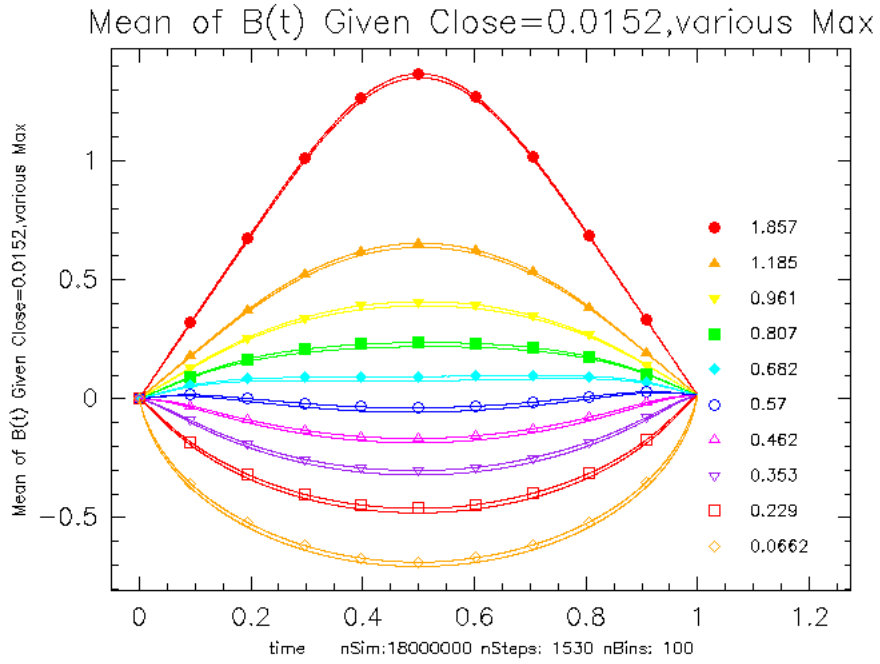


Figure 8: $E[B(t)|close = 0.0152, various high]$. The smooth curves with no symbol are given by (3.18) while the noisy curves are our simulation.

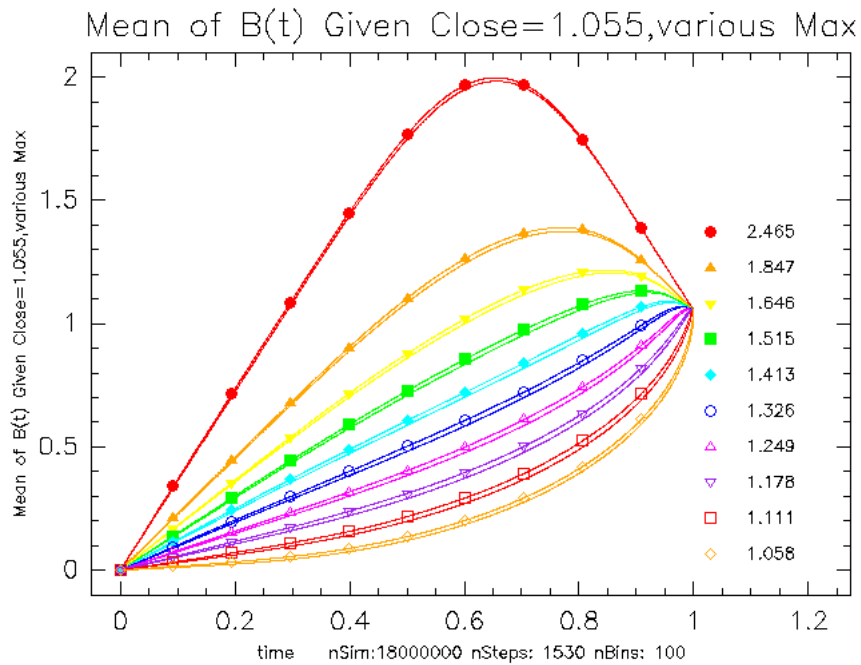


Figure 9: $E[B(t)|close = 1.055, various high]$. The values of the high are given in the legend.

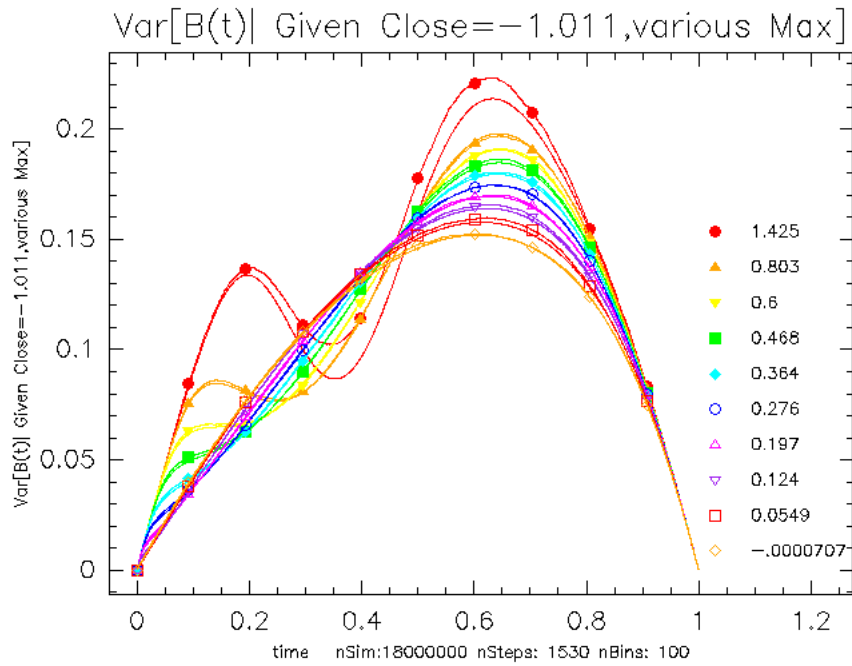


Figure 10: $Var[B(t|close = -1.011, high)]$.

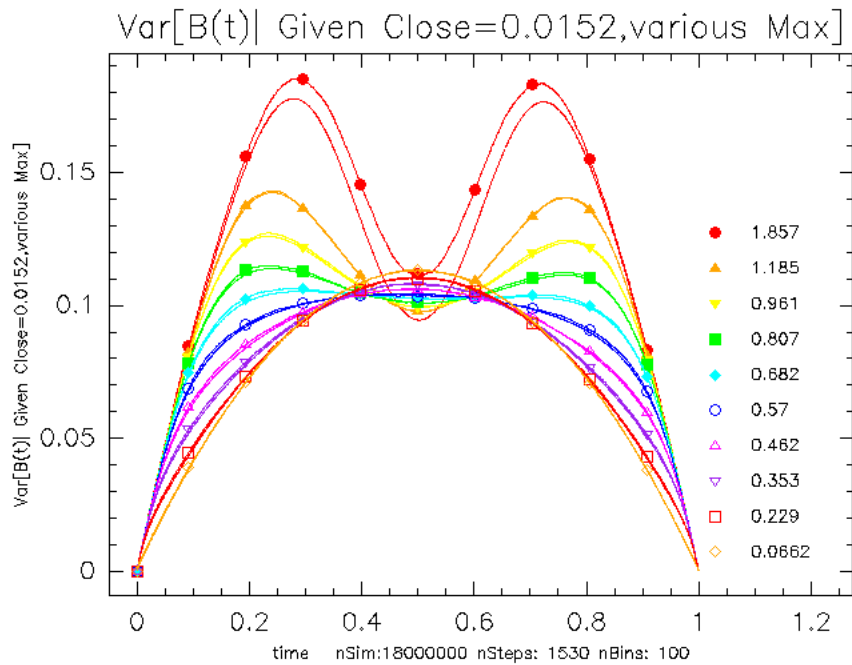


Figure 11: $Var[B(t|close = 0.0152, high)]$

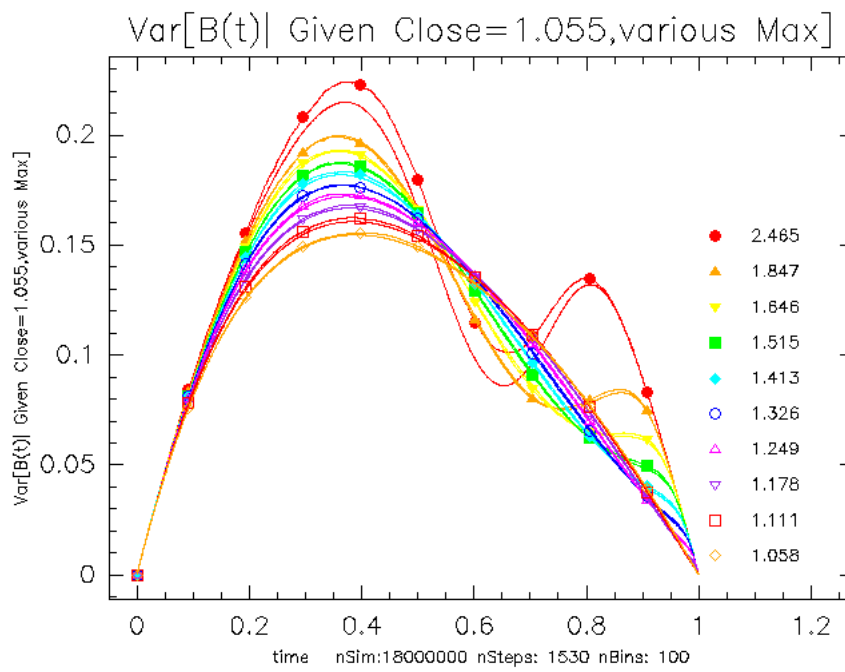


Figure 12: $Var[B(t|close = 1.055, high)]$

7 Comparison of Theory and Simulation Given Close and High

In this section, we plot the simulation and theoretical calculation given by (3.18) and (13.4). for this comparison, we use 30 million realizations each with 1530 steps. The results are then binned in 120 bins in each direction for a total of 1.73 million bins. We compute the MSE for each bin and sort them. We then display the fits for the worst .05, .02, .01 and .002 quantiles of the bins. To put the curves to scale, we plot all the curves together. The curves overstruck by symbols are the simulation curves. The analytic formula curves have the same color but no symbol. We now display the comparisons for each

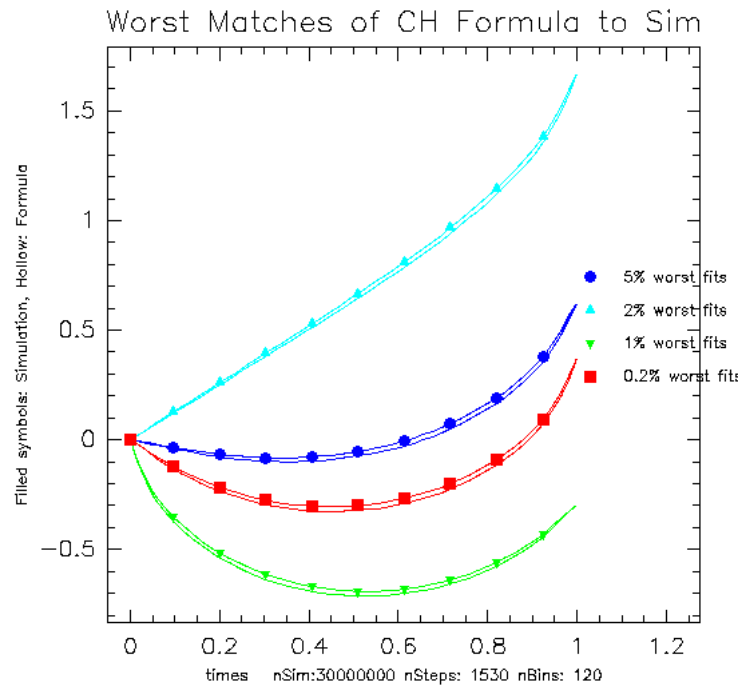


Figure 13: Comparison of simulation with (3.18) for four values of (c, h) . 5% worst MSE Mean:.0000117 at close:0.622, high:0.718 2% worst MSE Mean:.0000124 at close:1.67, high:1.739 1% worst MSE Mean:.000013 at close:-0.294, high:0.0581 0.2% worst MSE Mean:.0000136 at close:0.373, high:0.446

bin separately. This rescales the y-axis and makes the comparison look worse. The differences are due to a) averaging realizations for different values of (c, h) ; b) discretization errors from the finite time step of the Brownian motion. The black curve is the analytic expression while the blue curve is the the ensemble average of the simulation within the given bin. Figure 14 compares the simulated variance in four separate bins with the analytic expression in (13.4). Here again, we compute the squared error for each of the one million bins. We then plot the fits for the worst .05, .02, .01 and .002 quantiles of the bins. The worst fits for the variance have different parameters than the parameters for the worst fits to the empirical mean. To put the curves to scale, we plot all the curves together.

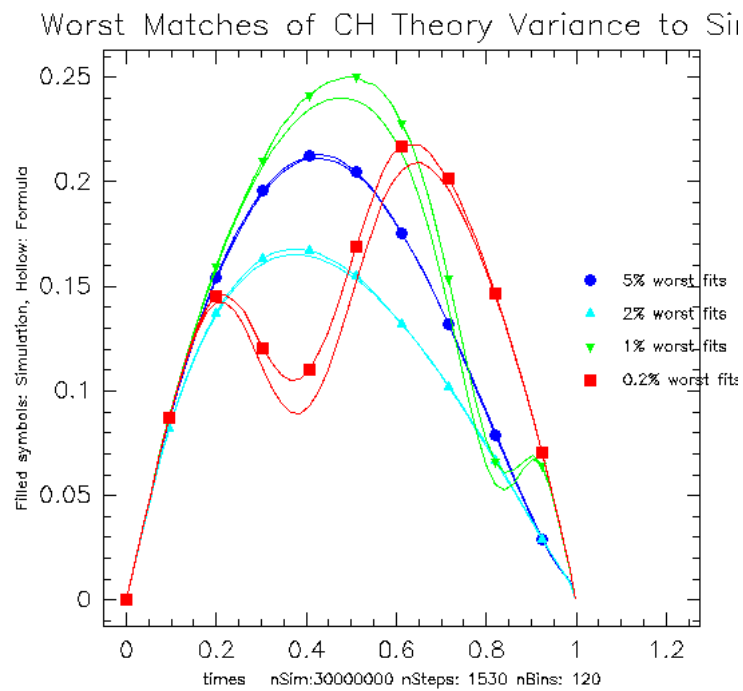


Figure 14: Comparison of simulation with (13.4) for four values of (c, h) . 5% worst MSE Var:.000000363 at close:1.996, high:2.167 2% worst MSE Var:.000000567 at close:1.007, high:1.148 1% worst MSE Var:.0000236 at close:3.125, high:4.036 0.2% worst MSE Var:.0000277 at close:-0.836, high:1.518

8 Density Given High, Low and Close

To derive the the density of $p(x; t, c, h, \ell)$, we need to consider four terms, the probability that both the high and low are to the left of t , the probability that just the low is to the left of t , the probability that just the high is to the right of t and the probability that both the high and the low are to the right of t .

$$P(x; t, h, \ell, c) \equiv P(B(t) = x | B(1) = c, \max\{B(s)\} = h, \min\{B(s)\} = \ell) = \tag{8.1}$$

$$P(t_\ell < t, t_h < t) + P(t_\ell < t, t_h \geq t) + P(t_\ell \geq t, t_h < t) + P(t_\ell \geq t, t_h \geq t) \tag{8.2}$$

where t_ℓ is the first time that B reaches its minimum. Applying (2.8) in the time interval $s \in [0, t]$ yields

$$P(B(t) = x, \ell \leq B(s) \leq h | s \leq t) = \sum_{j=-\infty}^{\infty} \left[\phi_t(x - 2j(h - \ell)) - \phi_t(x - 2h + 2j(h - \ell)) \right] \tag{8.3}$$

which we denote as $Q(x, t, h, \ell)$. Here ϕ_t denotes the Gaussian with variance t . The right term in (8.3) can be replaced by $\phi_t(x - 2h - 2j(h - \ell))$ or by $\phi_t(x - 2h + 2(j \pm 1)(h - \ell))$ and the equation remains valid. The shifted representation, $j \rightarrow j + 1$ is equivalent to $\phi_t(x - 2\ell + 2j(h - \ell))$. We define $G(x, t, h, \ell, c)$ by

$$G(x, t, h, \ell, c) \equiv P(B(t) = x, \ell \leq B(s) \leq h) P(B'(1 - t) = c - x, \ell - x \leq B'(s) \leq h - x | s \leq 1 - t) \tag{8.4}$$

where B' is a second Brownian motion defined for $s \leq 1 - t$. The density in (8.1) satisfies

$$P(x; t, h, \ell, c) = -\partial_\ell \partial_h G(x, t, h, \ell, c) . \tag{8.5}$$

Analogous to (3.2), equation (8.5) is the kernel of the Chapman-Kolmogorov representation for this restricted Brownian motion problem. The rightmost term in (8.4) has the representation:

$$P(B'(1 - t) = c - x, \ell - x \leq B'(s) \leq h - x) = \sum_{k=-\infty}^{\infty} \left[\phi_{1-t}(x - c + 2k\Delta) - \phi_{1-t}(x - (2h - c) - 2k\Delta) \right] \tag{8.6}$$

which we denote as $Q_R(x, t, h, \ell, c)$. Clearly, $Q_R(x, t, h, \ell, c) = Q(c - x, 1 - t, h - x, \ell - x)$. Δ is the high - low on $[0, 1]$, $\Delta \equiv h - \ell$. Δ is the expansion parameter for series convergence in (8.3) and (8.6). Luckily, our analysis of the Feller range in Section 5.3 shows that the set of small values of Δ is of very small measure.

As in (3.9), we decompose the generator, $G(x, t, h, \ell, c)$, into a sum of Gaussians in x .

$$G(x, t, h, \ell, c) \equiv \sum_{j,k>-\infty}^{\infty} \sum_{i=1}^4 \frac{s_i}{\sqrt{2\pi}} f_{ijk}(x) = \sum_{j,k>-\infty}^{\infty} \sum_{i=1}^4 \frac{s_i}{2\pi\sigma} \exp\left(-\frac{(x - a_{ij})^2}{2t} - \frac{(x - b_{ik})^2}{2(1-t)} \right) . \tag{8.7}$$

Here $\sigma^2 \equiv t(1-t)$, $a_{1,j} = 2j\Delta$, $b_{1,k} = c - 2k\Delta$, $a_{2,j} = 2j\Delta$, $b_{2,k} = 2h - c + 2k\Delta$, $a_{3,j} = 2h - 2j\Delta$, $b_{3,k} = c - 2k\Delta$, $a_{4,j} = 2h - 2j\Delta$, $b_{4,k} = 2h - c + 2k\Delta$. Note that $\sum_{i=1}^4 s_i f_{ijk}(x = h) = 0$. $\sum_{i=1}^4 s_i \partial_h f_{ijk}(x = h) = 0$ and $\sum_{i=1}^4 s_i \partial_l f_{ijk}(x = h) = 0$. This allows us to integrate by parts and drop terms.

We define $\mu_{ijk}(t, c, h) \equiv (a_{ij}(1-t) + b_{ik}t)$ and $g_i = ([a_{ij}^2(1-t) + tb_{ik}^2] - \mu_{ijk}^2) / (2\sigma^2) = (a_{ij} - b_{ik})^2 / 2$. Thus

$$G(x, t, h, \ell, c) = \sum_{j,k>-\infty}^{\infty} \sum_{i=1}^4 \frac{s_i}{\sqrt{2\pi}} \phi_{\sigma^2}(x - \mu_{ijk}(h, \ell)) e^{-g_{ijk}(h, \ell)} , \tag{8.8}$$

where ϕ_{σ^2} is once again the scaled Gaussian. Let $v_{j,k} = 2(j(1-t) + kt)$, $\tilde{v}_{j,k} = 2(j(1-t) - kt)$, $w_{j,k} = 2(j+k)$, $\tilde{w}_{j,k} = 2(j-k)$. Thus, $\mu_{1,j,k} = ct + \tilde{v}_{j,k}\Delta$, $g_1 = (c - w_{j,k}\Delta)^2 / 2$, $\mu_2 = (2h - c)t + v_{j,k}\Delta$, $g_2 = (2h - c - \tilde{w}_{j,k}\Delta)^2 / 2$, $\mu_3 = 2h(1-t) + ct - v_{j,k}\Delta$, $g_3 = (2h - c - \tilde{w}_{j,k}\Delta)^2 / 2$ and $\mu_4 = 2h - ct - \tilde{v}_{j,k}\Delta$, $g_4 = (c - w_{j,k}\Delta)^2 / 2$. In this section, we will often need the triple sum, $\sum_{j,k>-\infty}^{\infty} \sum_{i=1}^4$. For notational simplicity, we replace the triple sum with a simple \sum_{ijk} when appropriate.

We define the moments M_m where the limits of integration, H and L , are to be set to h and ℓ after we differentiate $\partial_h \partial_\ell G$.

$$M_m(t, h, \ell, c) \equiv - \int_L^H x^m \partial_h \partial_\ell G(x, t, h, \ell, c) = \int_L^H x^m \sum_{j,k > -\infty}^{\infty} \sum_{i=1}^4 \frac{-s_i}{\sqrt{2\pi}} \partial_h \partial_\ell f_{ijk}(x, h, \ell) . \quad (8.9)$$

The (i, j, k) th term inside the integral satisfies

$$- \partial_h \partial_\ell \phi_{\sigma^2}(x - \mu_{ijk}(t, h, \ell)) e^{-g_{ijk}(h, \ell, t)} = H_{ijk}(x - \mu_{ijk}) \phi_{\sigma^2}(x - \mu_{ijk}(t, h, \ell)) e^{-g_{ijk}} . \quad (8.10)$$

Here $H_{ijk}(z)$ is defined as

$$H_{ijk}(z) \equiv - \left[\frac{z \tau_{ijk}}{\sigma^2} - \partial_h g_{ijk} \right] \left[\frac{z \hat{\tau}_{ijk}}{\sigma^2} - \partial_\ell g_{ijk} \right] + \frac{\tau_{ijk} \hat{\tau}_{ijk}}{\sigma^2} + \partial_\ell \partial_h g_{ijk} . \quad (8.11)$$

where $\tau_{ijk} \equiv \partial_h \mu_{ijk}$ and $\hat{\tau}_{ijk} \equiv \partial_\ell \mu_{ijk}$. Thus $\tau_{1jk} = \tilde{v}_{j,k} = -\hat{\tau}_{1jk}$, $\tau_{2jk} = 2t + v_{j,k}$, $\hat{\tau}_{2jk} = -v_{j,k}$, $\tau_{3jk} = 2(1-t) - v_{j,k}$, $\hat{\tau}_{3jk} = v_{j,k}$, $\tau_{4jk} = 2 - \tilde{v}_{j,k}$ and $\hat{\tau}_{4jk} = \tilde{v}_{j,k}$. Note that τ and $\hat{\tau}$ have no dependence on h and ℓ . We group the terms in (8.11) by powers of z and define $A_{ijk} = \tau_{ijk} \hat{\tau}_{ijk}$, $B_{ijk} = [\tau_{ijk} \partial_\ell g_{ijk} + \hat{\tau}_{ijk} \partial_h g_{ijk}]$ and $C_{ijk} = \Gamma_{ijk} + \sigma^{-2} \tau_{ijk} \hat{\tau}_{ijk}$ and $\Gamma_{ijk} \equiv -\partial_h g_{ijk} \partial_\ell g_{ijk} + \partial_\ell \partial_h g_{ijk}$. Thus $H_{ijk}(z) = -A_{ijk} z^2 / \sigma^4 + B_{ijk} z / \sigma^2 + C_{ijk}$. To simplify the moment calculation, we evaluate the derivatives by h and ℓ and recast them as derivatives with respect to x so that we can integrate by parts:

$$\partial_h \partial_\ell f_{ijk} = \tau_{ijk} \hat{\tau}_{ijk} \partial_x^2 f_{ijk} + B_{ijk} \partial_x f_{ijk} - \Gamma_{ijk} f_{ijk} . \quad (8.12)$$

We integrate by parts and find from (8.12):

$$M_m(t, h, \ell, c) = \sum_{j,k > -\infty}^{\infty} \sum_{i=1}^4 \frac{s_i}{\sqrt{2\pi}} \int_L^H m x^{m-1} [A_{ijk} \partial_x f_{ijk} + B_{ijk} f_{ijk}] + x^m \Gamma_{ijk} f_{ijk} \quad (8.13)$$

$$+ \sum_{i,j,k} \frac{\mathcal{B}_{ijk}(x=h) - \mathcal{B}_{ijk}(x=\ell)}{\sqrt{2\pi}}$$

where \mathcal{B}_{ijk} is the boundary term. In the Appendix, we show that the boundary terms sum to zero. Also in the Appendix, we define the functions $G_{mn}()$. We then have the representation:

$$M_m(h, \ell) = \sum_{ijk} \frac{s_i}{\sqrt{2\pi}} \left[\frac{-mA_{ijk}}{\sigma^2} G_{m-1,1}(\mu_{ijk}) + mB_{ijk} G_{m-1,0}(\mu_{ijk}) + \Gamma_{ijk} G_{m0}(\mu_{ijk}) \right] e^{-g_{ijk}} . \quad (8.14)$$

For M_0 , only the last term is nonzero and the sum reduces to

$$M_0 = \sum_{ijk} \frac{s_i}{\sqrt{2\pi}} \Gamma_{ijk} e^{-g_{ijk}} [E_\sigma(h - \mu_{ijk}) - E_\sigma(\ell - \mu_{ijk})]$$

$$= \sum_{jk} \sum_{i=1}^2 \frac{s_i}{\sqrt{2\pi}} \Gamma_{ijk} e^{-g_{ijk}} [E_\sigma(\ell - \mu_{ijk} + 2\Delta) - E_\sigma(\ell - \mu_{ijk})] .$$

To simplify the first sum, we used $h - \mu_{4jk} = \mu_{1jk} - h$, $h - \mu_{3jk} = \mu_{2jk} - h$, $E_\sigma(\ell - \mu_{4jk}) = -E_\sigma(\ell - \mu_{1jk} + 2\Delta)$, $E_\sigma(\ell - \mu_{3jk}) = -E_\sigma(\ell - \mu_{2jk} + 2\Delta)$. The Γ_{ijk} satisfy $\Gamma_{1jk} = (2g_{1jk} - 1)w_{jk}^2 = w_{jk}^2[(c - w_{j,k}\Delta)^2 - 1]$ and $\Gamma_{2jk} = (2g_{2jk} - 1)\tilde{w}_{jk}(\tilde{w}_{jk} - 2) = \tilde{w}_{jk}\tilde{w}_{j,k+1}[(2h - c - \tilde{w}_{j,k}\Delta)^2 - 1]$.

To sum these terms, we reparametrize $k(j, \hat{k})$. For $i = 1, 4$, we set $k = \hat{k} - j$, $\hat{k} = k + j$. For $i = 2, 3$, we set $k = j - \hat{k}$, $\hat{k} = k - j$. With these transformations, $v_{j,\hat{k}} = j - \hat{k}t$, $\tilde{v}_{j,\hat{k}} = j - \hat{k}t$, $w_{j,\hat{k}} = 2\hat{k}$, $\tilde{w}_{j,\hat{k}} = 2\hat{k}$, $\mu_{1,j\hat{k}} = ct + \tilde{v}_{j,\hat{k}}\Delta$, $g_1 = (c - w_{j,\hat{k}}\Delta)^2/2$, $\mu_2 = (2h - c)t + v_{j,\hat{k}}\Delta$, $g_2 = (2h - c - \tilde{w}_{j,\hat{k}}\Delta)^2/2$. Since the g_i depend only on \hat{k} and not j , so do the $\Gamma_{j\hat{k}}$. The double sum splits into a single sum

$$\sum_{i\hat{k}} \Gamma_{i\hat{k}} e^{-g_{i\hat{k}}} \sum_j [E_\sigma(\ell - \mu_{i\hat{k}} + 2\Delta) - E_\sigma(\ell - \mu_{i\hat{k}})] = \sum_{\hat{k}} \Gamma_{1\hat{k}} e^{-g_{1\hat{k}}} - \Gamma_{2\hat{k}} e^{-g_{2\hat{k}}} \quad (8.15)$$

where we have dropped the j dependence on g and Γ . We use that for a given k , the sum of the integrals for $(1, j, \hat{k})$ and $(4, j, \hat{k})$ cover the region from $-\infty$ to ∞ . This allows us to collapse the sum over $i \in (1, 4), j$. Similarly, the sums over $(2, j, \hat{k})$ and $(3, j, \hat{k})$ collapse. We recognize the expression in (8.15) to precisely correspond to $M_0(t, h, \ell, c) = p(h, \ell, c)$ as given by (2.10).

We would very much like to have expressions for the first and second moment that reduce the double sum to a single sum. This does not appear possible because the a_{ijk} and a'_{ijk} do not vanish. For $m \leq 2$, equation (8.14) becomes

$$M_m(t) = \sum_{ijk} \frac{s_i e^{-g_{ijk}}}{\sqrt{2\pi}} \left[a_{ijk}^{(m)} \phi_{\sigma^2}(h - \mu_{ijk}) - \hat{a}_{ijk}^{(m)} \phi_{\sigma^2}(\ell - \mu_{ijk}) + e_{ijk}^{(m)} R_{\sigma}(h, \ell, \mu_{ijk}) \right], \quad (8.16)$$

where $R_{\sigma}(h, \ell, \mu_{ijk}) \equiv [E_{\sigma}(h - \mu_{ijk}) - E_{\sigma}(\ell - \mu_{ijk})]$. When $m > 2$, the terms multiplying $E_{\sigma}(h - \mu_{ijk})$ and $E_{\sigma}(\ell - \mu_{ijk})$ may be different. For $m = 1$, the coefficients are

$$a_{ijk}^{(1)} = \hat{a}_{ijk}^{(1)} = A_{ijk} - \Gamma_{ijk} * \sigma^2, \quad e_{ijk}^{(1)} = B_{ijk} + \Gamma_{ijk} \mu_{ijk}. \quad (8.17)$$

For $m = 2$, the coefficients are

$$\begin{aligned} a_{ijk}^{(2)} &= 2hA_{ijk} + 2B_{ijk}\sigma^2 + \Gamma_{ijk}\sigma^2(\mu_{ijk} + h), \\ \hat{a}_{ijk}^{(2)} &= 2\ell A_{ijk} + 2B_{ijk}\sigma^2 + \Gamma_{ijk}\sigma^2(\mu_{ijk} + \ell), \\ e_{ijk}^{(2)} &= 2B_{ijk}\mu_{ijk} - 2A_{ijk} + \Gamma_{ijk} * (\mu_{ijk}^2 + \sigma^2). \end{aligned} \quad (8.18)$$

For $m = 0$, $a_{ijk}^{(0)} = \hat{a}_{ijk}^{(0)} = 0$ and $e_{ijk}^{(0)} = \Gamma_{ijk}$. In the Appendix, we further simplify the expressions in (8.16)-(8.17). We are unable to collapse the two dimensional sum over j and k to a single infinite sum as was possible in the $m = 0$ case.

To evaluate (8.14) numerically, we need to truncate the expansion in j and k . Luckily, the Feller distribution of 5.3 shows that very few realizations have small values of Δ . Thus the double expansion for j and k converges quickly for the vast majority of the Brownian realizations.

A second method to evaluate the probability of (8.1) is to define $Q(x, t, h, \ell, c) \equiv P(B(t) = x, \ell \leq B(t) \leq h)$ by (8.3) and to numerically evaluate Q , $\partial_h Q$, $\partial_{\ell} Q$ and $\partial_{\ell} \partial_h Q$. Similarly, we define $Q_R(x, t, h, \ell, c) \equiv P(B(1-t) = c - x, \ell - c \leq B(s) \leq h - c)$ by (8.6) and numerically evaluate Q_R , $\partial_h Q_R$, $\partial_{\ell} Q_R$ and $\partial_{\ell} \partial_h Q_R$. We then numerically integrate the moments of (8.19).

$$prob(x, t, h, \ell, c) = Q(x, t, h, \ell) \partial_{\ell} \partial_h Q_R + \partial_h Q(x, t, h, \ell) \partial_{\ell} Q_R + \partial_{\ell} Q \partial_h Q_R + Q \partial_{\ell} \partial_h Q_R(x, t, h, \ell, c) \quad (8.19)$$

times x^m from $x = \ell$ to $x = h$. Each of the terms in the integral involves truncating only in one of j or k . Thus the additional work involved in evaluating Q and Q_R at many points to evaluate the integral is partially compensated by the single infinite sums as opposed to a doubly infinite sum.

9 Figures Conditional on Close, High, Low

In this section, we plot the $E[B(t|c, h, \ell)]$ and $Var[B(t|c, h, \ell)]$ for a variety of different values of (c, h, ℓ) . Specifically, we choose quantiles (.2, .5, .8) of the bin values for the close. For our robustified grid, this corresponds to $close = -1.011, 0.0152, 1.055$. For each value of the close, we choose three values for the high corresponding to the (.2, .5, .8) quantiles of the robustified grid in h . This gives nine plots for $E[B(t|c, h, \ell)]$. In each plot, we plot the expectation $E[B(t|c, h, \ell)]$ for ten values of ℓ . We then repeat for $Var[B(t|c, h, \ell)]$. For these plots, we use 1530 time steps on each simulation for a total of 18 million simulations with 100 bins in each parameter direction. The curves overstruck by symbols are the simulation curves. The analytic formula curves have the same color but no symbol.

9.1 Time Dependent Mean Given Close, High, Low

Figures 15- 17 show $E[B(t|c, h, \ell)]$ for $c = -1.011$. Note that maximum of the expectation is less the expectation of the maximum. The curves on the three plots have a similar shape as the value of the low is varied. This may indicate a somewhat weaker dependence on high than on the low when the close equals -1. However, a stronger factor is that the curves in 'low' the low coordinate vary more since we sample 10 values from the second smallest bin value of ℓ to the second largest value of ℓ given (c, h) .

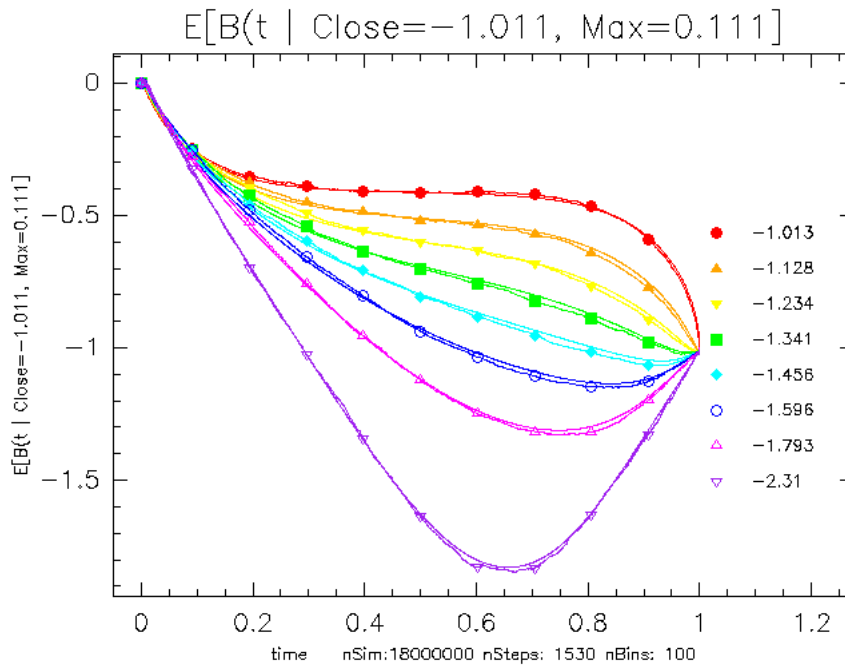


Figure 15: $E[B(t|close = -1.011, high = .111, various low)]$ where the values of the low are given in the legend. Smaller values of the low occur on average earlier in time.

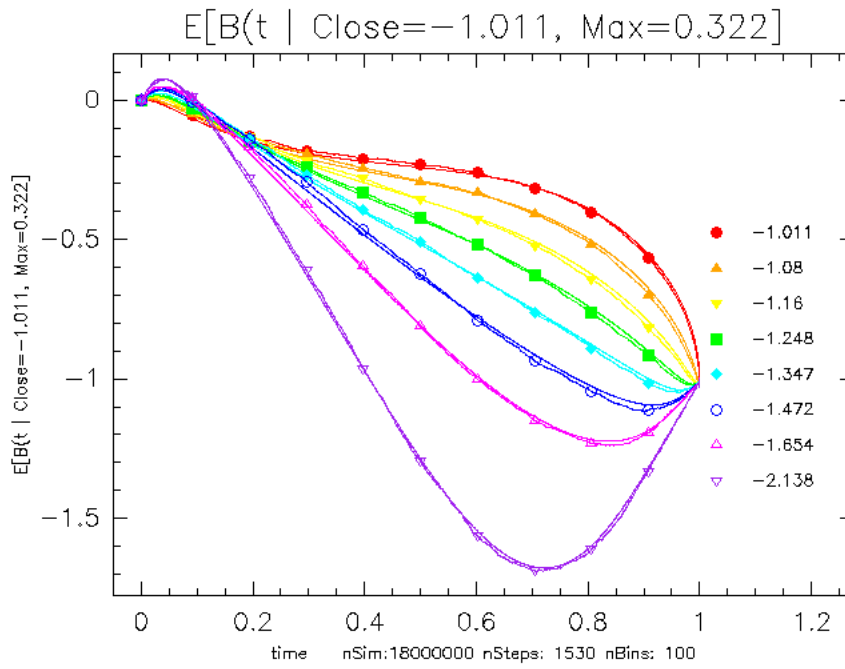


Figure 16: $E[B(t)|close = -1.011, high = 0.322, various low]$

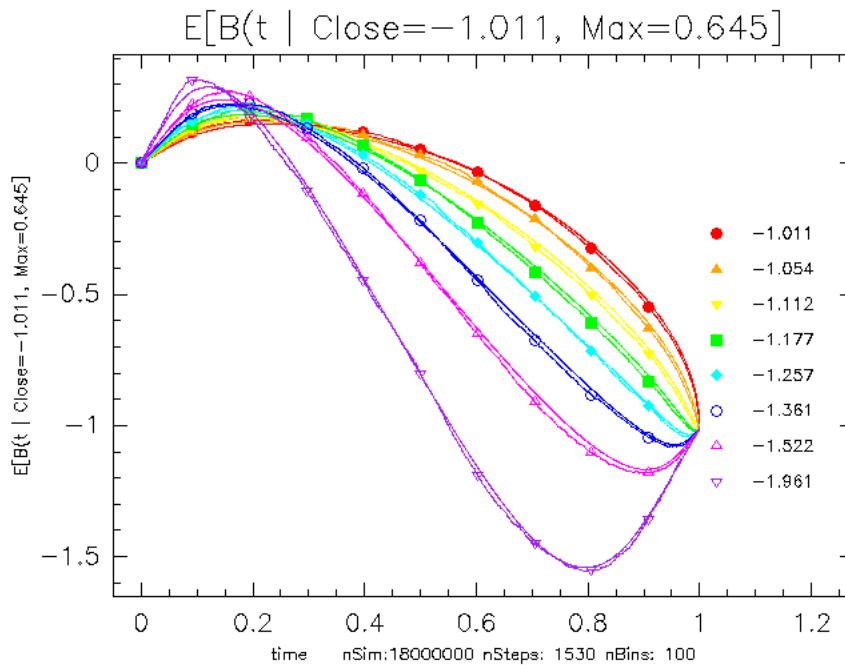


Figure 17: $E[B(t)|close = -1.011, high = 0.645, various low]$. The values of the minimum are given in the legend.

High, Low and Close in Brownian Estimation

Figures 18-20 show $close = 0.0152$. In this case ($close$ near zero), the expectation is roughly symmetric. In Figure 20, the curves for large high and small low are not very symmetric, but this may be due to fewer curves in the bin due to our adaptive binning. We have also plotted $E[B(t|c, h, \ell)]$ for $c \approx 1$. These

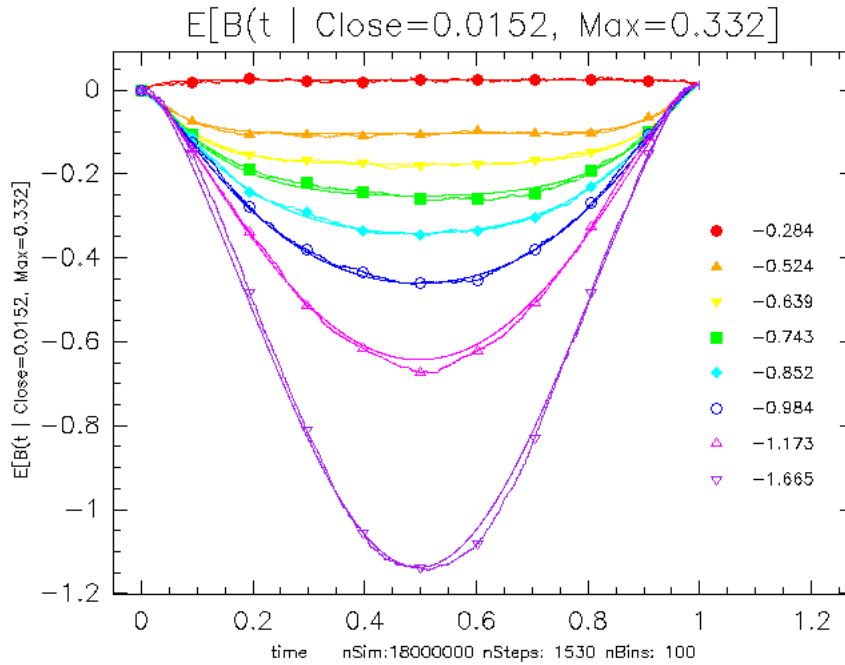


Figure 18: $E[B(t|close = 0.0152, high = 0.332, various\ low)]$

plots exhibit the same reflection symmetry that Figure 7 and Figure 9 do. Specifically, the reflection symmetry: $E[B(t | -c, h, \ell)] = E[B(1 - t|c, h + c, \ell + c)] - c$ where $c > 0$.

High, Low and Close in Brownian Estimation

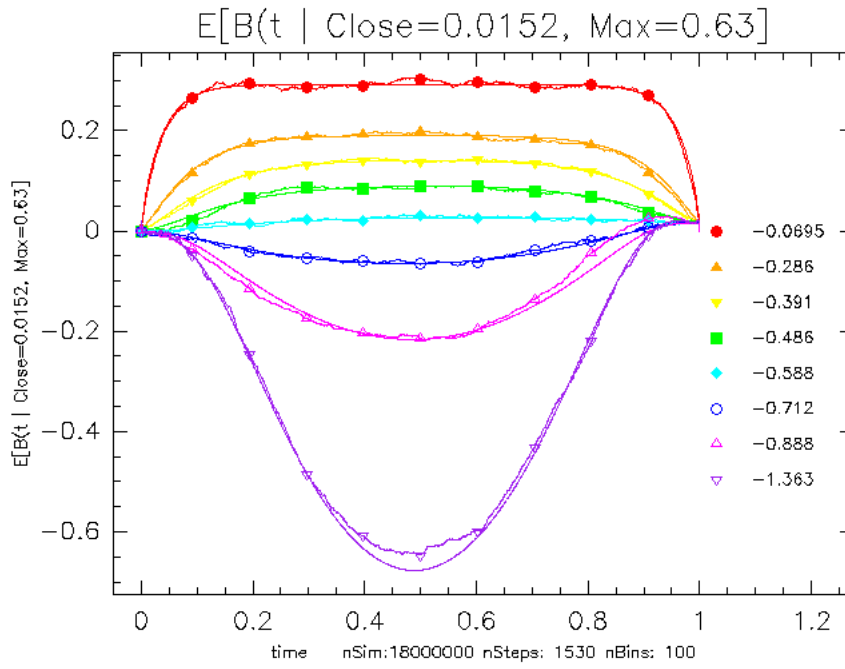


Figure 19: $E[B(t)|\text{close} = 0.0152, \text{high} = 0.63, \text{various low}]$

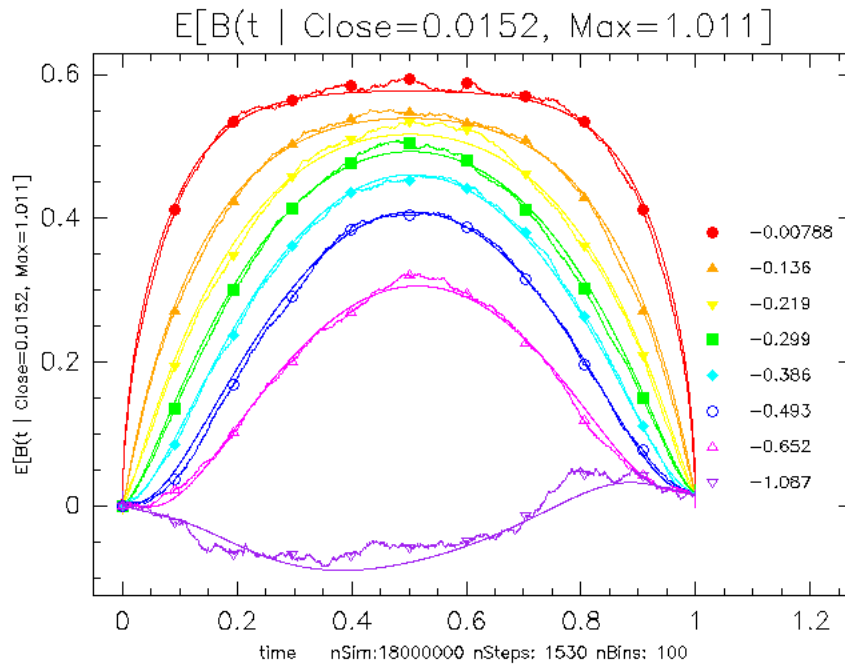


Figure 20: $E[B(t)|\text{close} = 0.0152, \text{high} = 1.011, \text{various low}]$

9.2 Time Dependent Variance Given Close, High, Low

Figures 21-26 plot the $Var[B(t|c, h, \ell)]$ for $close = -1.011, 0.0152, 1.055$. For each value of the close, we choose we choose quantiles (.2,.5, .8) of the bin values for the high. In many cases, the variance is multimodal in time. The curves are much noisier because the 18 million realizations are now put into 10,000 bins instead of 100 bins.

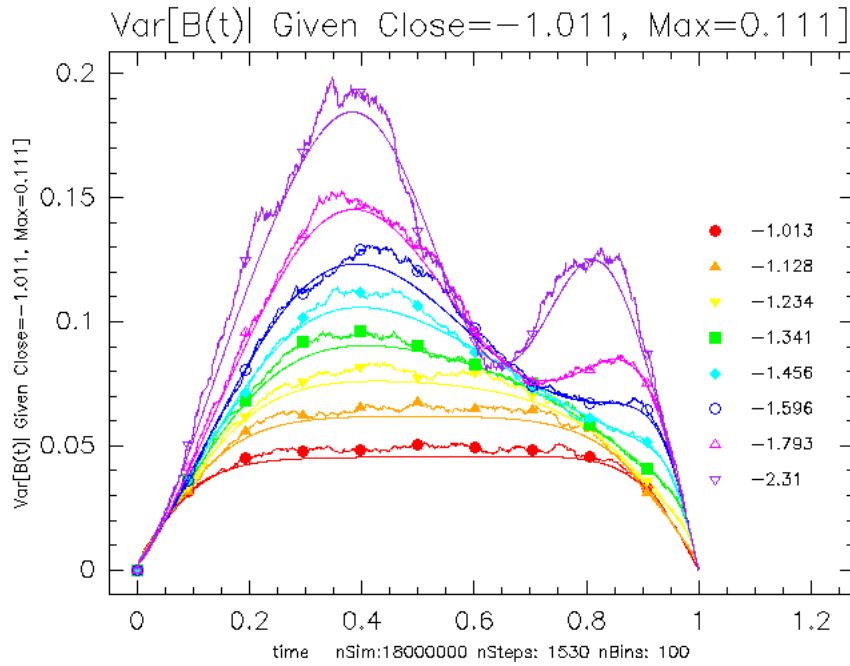


Figure 21: $Var[B(t|close = -1.011, high = 0.111, low)]$. The curves are roughly symmetric in time for small $|low|$ and multimodal for large $|low|$.

Figures 24-26 display the empirical variance when the close is near zero. In many cases, the variance is strongly bimodal with maxima near $t = .25$ and $t = .75$. The y -axis is self-scaled. The largest uncertainties occur for c near zero. Similarly, $Var[B(t|c, h, \ell)]$ for $c \approx 1$. These plots exhibit the same reflection symmetry that Figure 10 and Figure 12 do/ Specifically, the reflection symmetry: $Var[B(t - c, h, \ell)] = Var[B(1 - t|c, h + c, \ell + c)]$ where $c > 0$.

High, Low and Close in Brownian Estimation

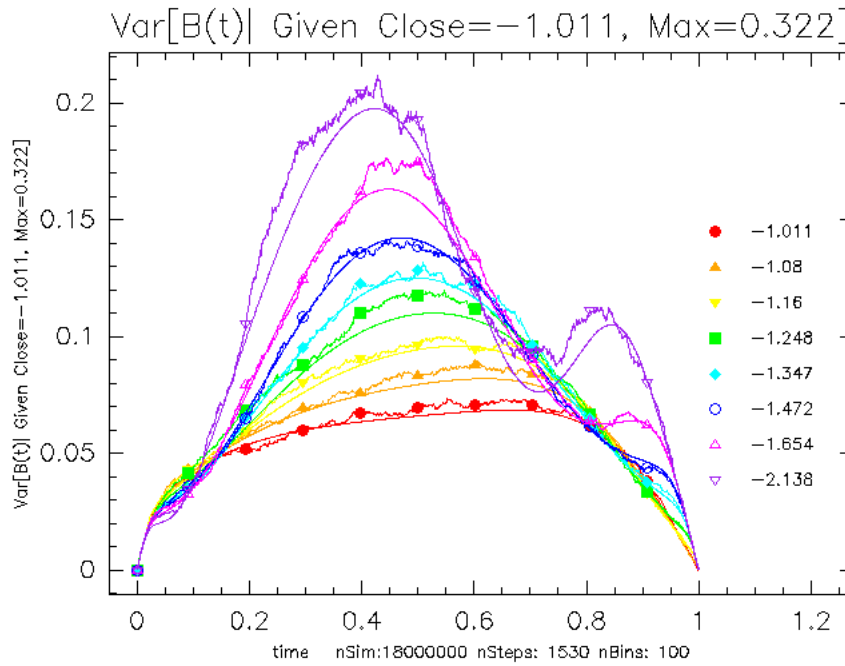


Figure 22: $Var[B(t)|close = -1.011, high = 0.322, low]$

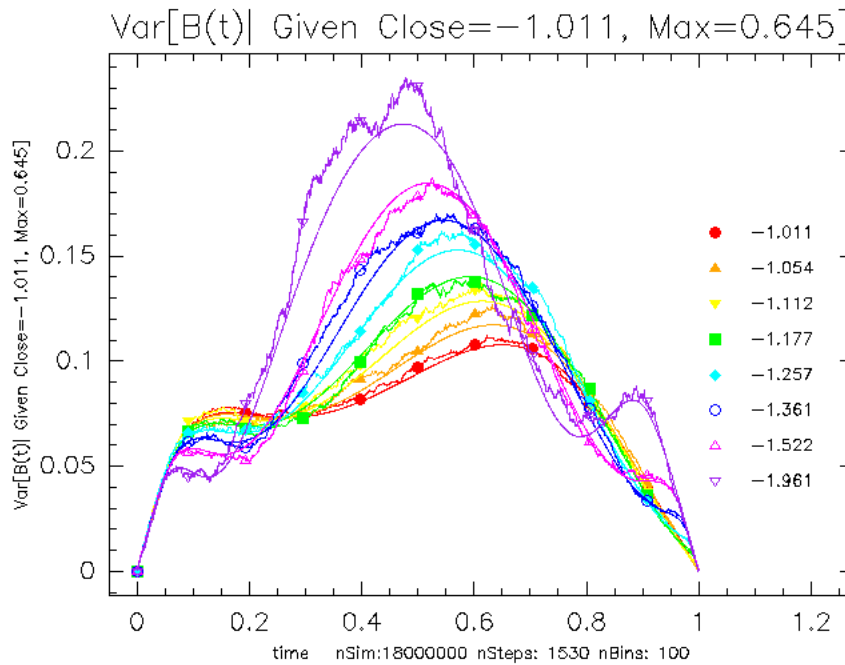


Figure 23: $Var[B(t)|close = -1.011, high = 0.645, low]$

High, Low and Close in Brownian Estimation

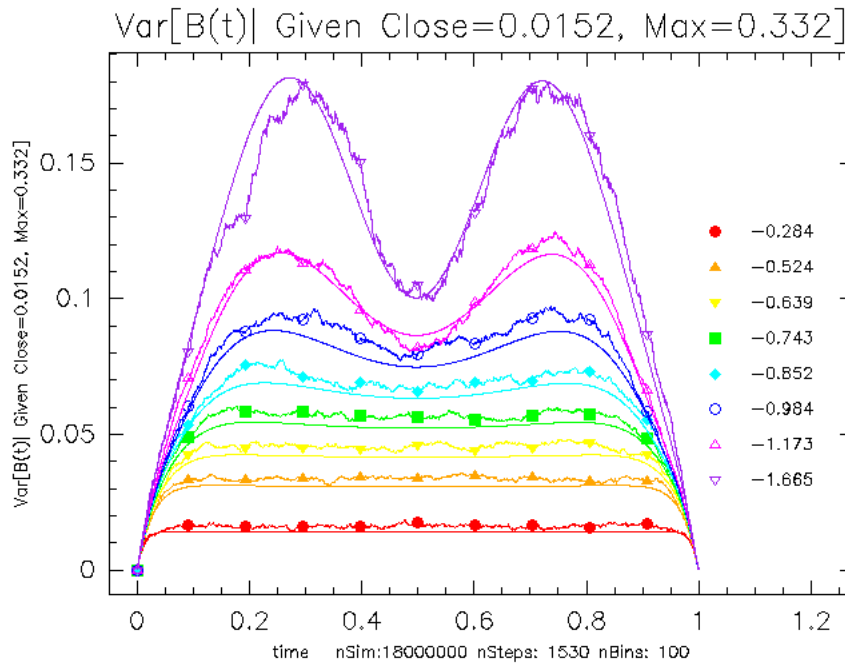


Figure 24: $Var[B(t|close = 0.0152, high =: 0.332, low)]$:VarGivenClose0.0152 Max0.332CHL

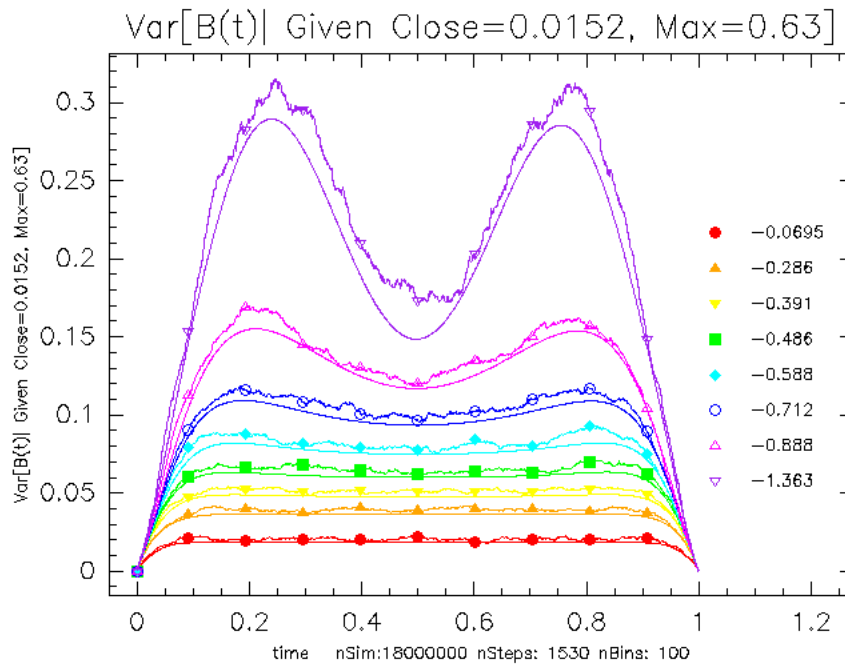


Figure 25: $Var[B(t|close = 0.0152, high = 0.63, low)]$

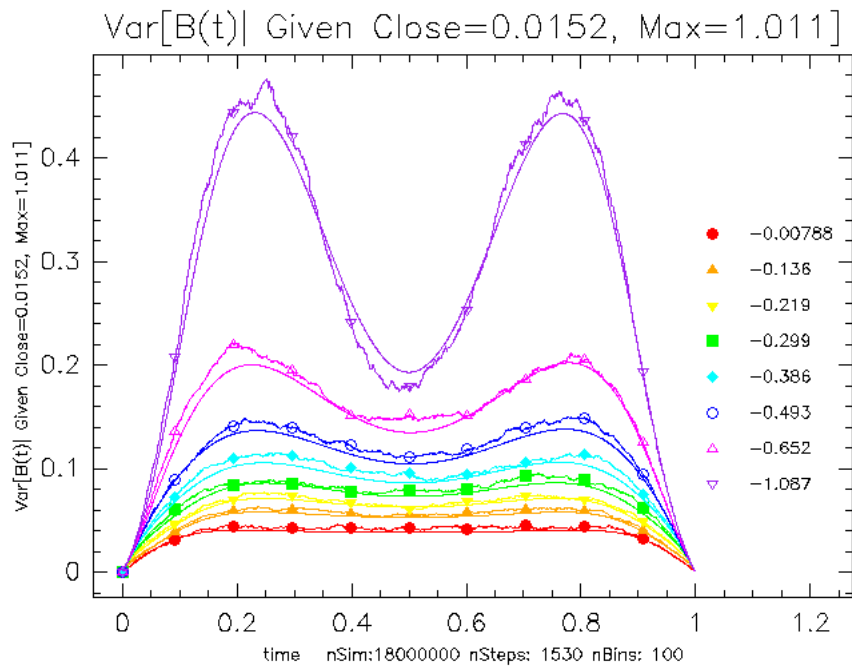


Figure 26: $Var[B(t)|close = 0.0152, high = 1.011, low]$

10 Comparison of Theory and Simulation Given Close, High and Low

In this section, we plot the simulation and theoretical calculation given by (8.14). For this comparison, we use 30 million realizations each with 1530 steps. The results are then binned in 120 bins in each direction, thus a total of 1.73 million bins. We compute the MSE for each bin and sort them. We then display the fits for the worst .05, .02, .01 and .002 of the bins. To put the curves to scale, we plot all the curves together.

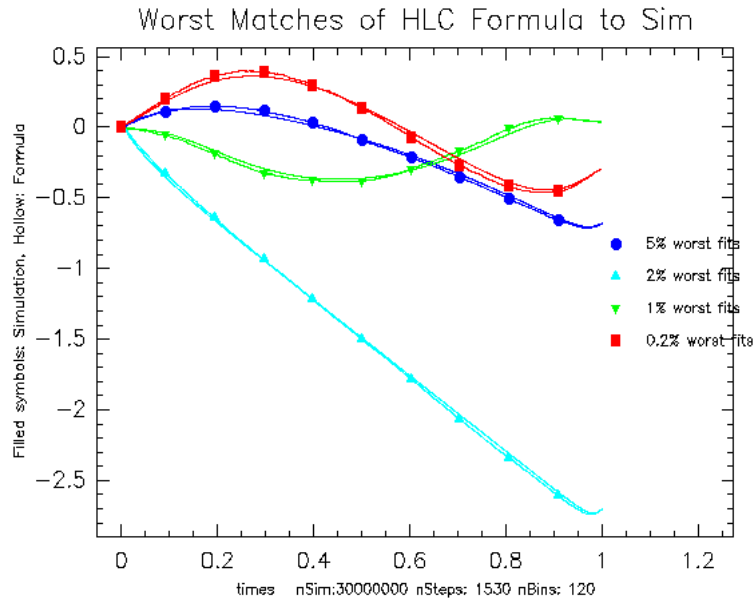


Figure 27: Comparison of simulation with (8.14) for four values of (c, h, ℓ) . 5% worst MSE Mean:.0000114 at close:-1.289, high:0.109, low:-1.502; 2% worst MSE Mean:.000014 at close:0.836, high:0.932, low:-0.487; 1% worst MSE Mean:.0000165 at close:0.972, high:1.256, low:-1.198; 0.2% worst MSE Mean:.0000257 at close:0.242, high:0.875, low:-1.056.

Figure 28 compares the simulated variance in four separate bins with the analytic expression in (13.4). Here again, we compute the squared error for each of the 1.73 million bins. We then plot the fits for the worst .05, .02, .01 and .002 quantiles of the bins. The worst fits for the variance have different parameters than the parameters for the worst fits to the empirical mean. To put the curves to scale, we plot all the curves together.

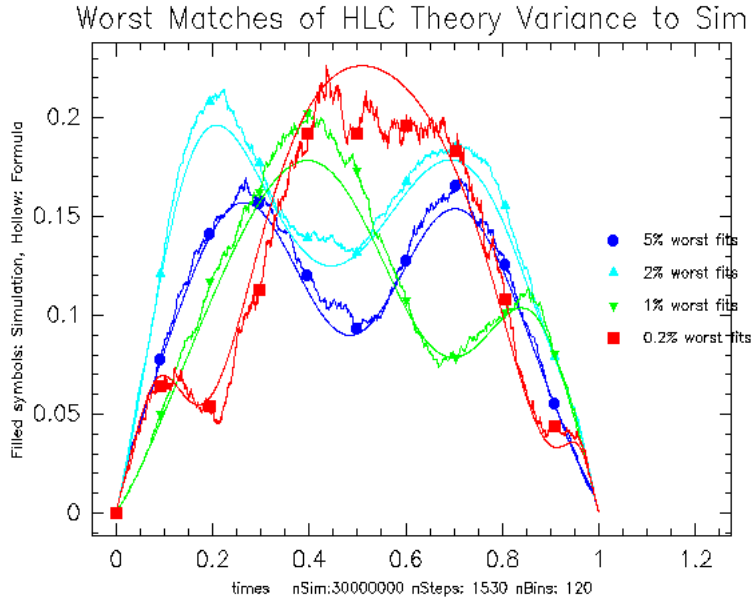


Figure 28: Comparison of simulation with (8.14) for four values of (c, h, ℓ) . 5% worst MSE Var:.00000124 at close:-0.038, high:0.756, low:-0.611; 2% worst MSE Var:.0000021 at close:3.125, high:3.286, low:-0.276; 1% worst MSE Var:.00000311 at close:-3.125, high:0.307, low:-3.642; 0.2% worst MSE Var:.00000695 at close:-3.125, high:0.911, low:-3.211.

11 Distribution Given High and Low

We evaluate the distribution $p(x, t, h, \ell)$ by integrating over the closing value in $p(x, t, h, \ell, c)$ using 8.7. As before, the limits of integration, H and L , are to be set to h and ℓ after differentiation. The generating function is

$$G_{HL}(x, t, h, \ell) \equiv \int_L^H G(x, t, h, \ell, c)dc = Q(x, t, h, \ell) \sum_{k>-\infty}^{\infty} [R_{1k}(x, t, h, \ell; H, L) - R_{2k}(x, t, h, \ell)] \quad (11.1)$$

where $Q(x, t, h, \ell)$ is defined in (8.3) and

$$R_{1k} = \frac{1}{2} \left[\operatorname{erf}\left(\frac{H-x-k\Delta}{\sqrt{2(1-t)}}\right) - \operatorname{erf}\left(\frac{L-x-k\Delta}{\sqrt{2(1-t)}}\right) \right],$$

$$R_{2k} = \frac{1}{2} \left[\operatorname{erf}\left(\frac{H+x-2h+k\Delta}{\sqrt{2(1-t)}}\right) - \operatorname{erf}\left(\frac{L+x-2h+k\Delta}{\sqrt{2(1-t)}}\right) \right].$$

The density satisfies $P(x; t, h, \ell) = -\partial_\ell \partial_h G(x, t, h, \ell; H, L)$. To get the density conditional on the high and low, we divide $P(x; t, h, \ell)$ by $p(h, \ell)$ as given by (2.11) The theoretical values of $E[B(t)|h, \ell]$ and $Var[B(t)|h, \ell]$ can be calculated by computing moments with respect to (5.1). Unfortunately, we have not found a tractable analytic form from the integrals and therefore we compute them numerically. We display the simulation results for $E[B(t)|h, \ell]$ for a small value of $h = .304$, the median value of $h = .816$ and a large value of $h = 1.572$.

High, Low and Close in Brownian Estimation

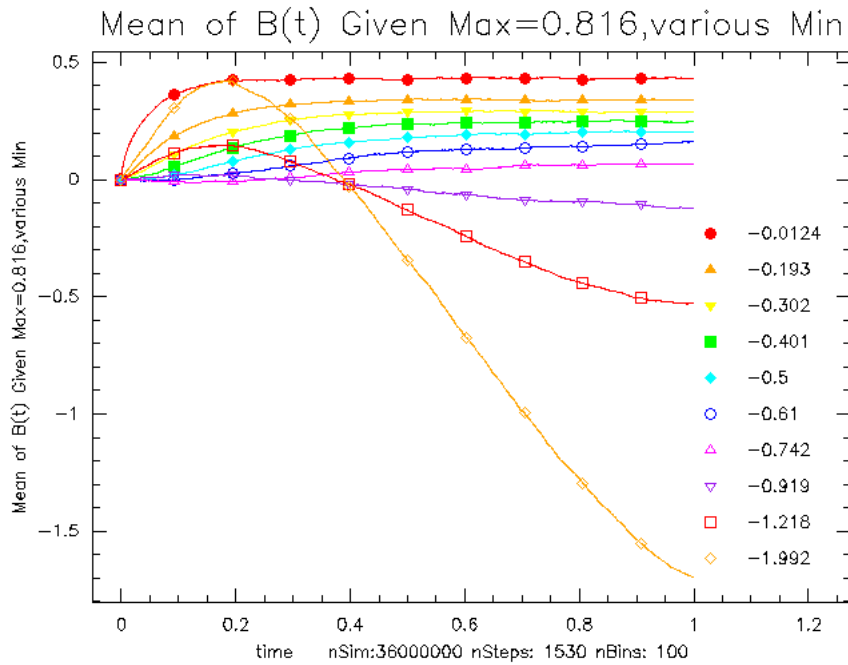
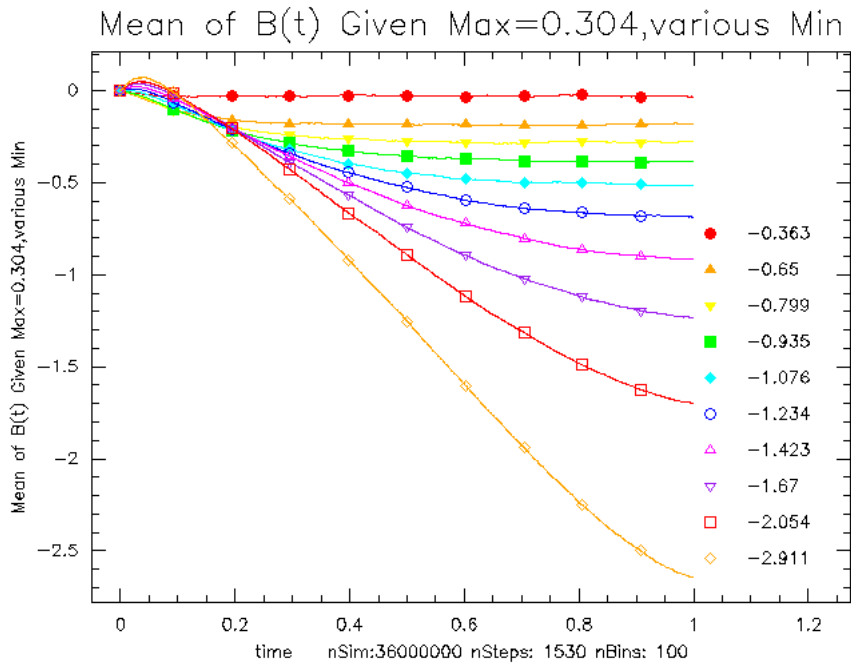


Figure 29: $E[B(t)|high = 0.816, \text{various low}]$. If the $h > |\ell|$, the maximum occurs after the minimum. If the $h < |\ell|$, the minimum occurs first.

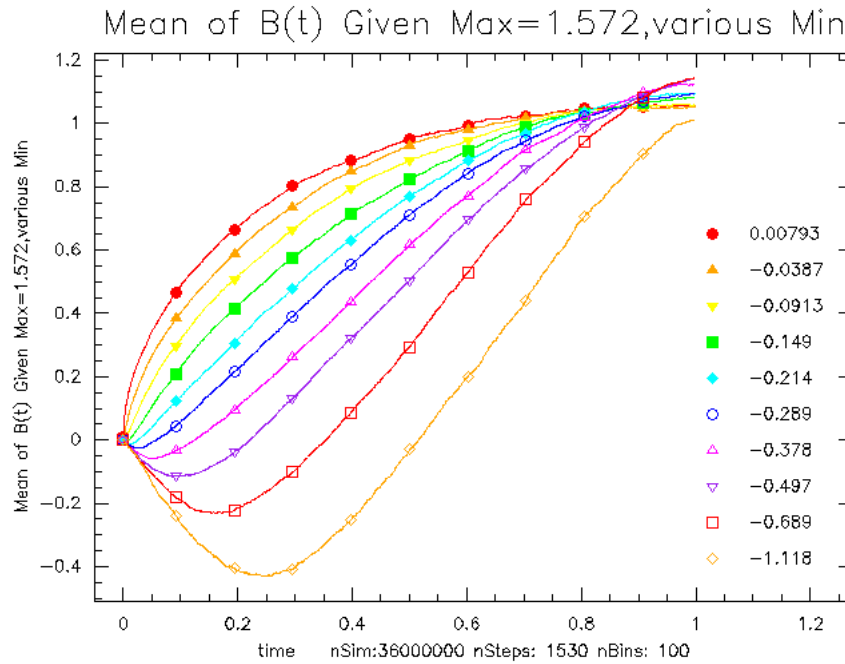


Figure 30: $E[B(t)|high = 1.572, various low]$

12 Summary

By calculating $E[B(t)]$ max, min, close], we are able to interpolate in time any dataset where only the open, high, low and close are given. In practice, we interpolate on the log scale using the logarithms of the open, high, low and close. For most applications, we are interested in relative price changes so the log scale is appropriate. If one is truly interested in the actual price, our formulas need to be modified for log Brownian motion.

Our simulations have calculated the ensemble average of the mean square error in Brownian motion for a variety of different givens. The time dependence of the variance is displayed in Figure 31. The variance is symmetric in time when final value is specified. If just the high or the high and low are specified, the variance is nonmonotonic in time. The time averaged variance is displayed in Table 1. It is slightly better to know the high than the closing value. It is better to know the close and the high than the close and time of the high. It is better to know the close, high and low than to know the close high and time of the high. The values for Table 1 and Figure 31 are from the simulation. We plan to compute these ensemble averages using the analytic results in Sections 3 and 8.

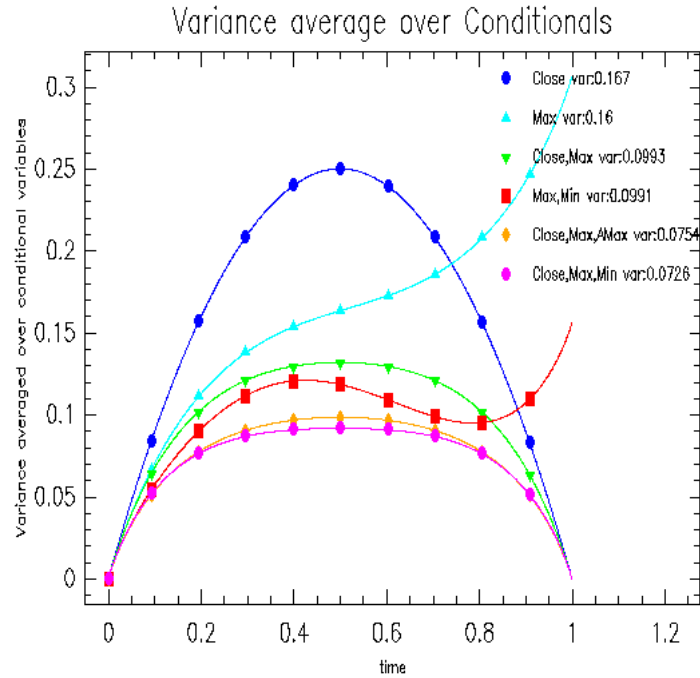


Figure 31: Time Dependence of Ensemble Averaged Variance Given Conditional Variables

Table 1: Time Averaged Variance by Givens

| Givens | Var | Var*6 |
|---------------------|---------|--------|
| Start point only | 1/2 | 3 |
| Close | 1/6 | 1 |
| High | 0.1602 | .9612 |
| ArgMax | .2487 | 1.492 |
| Close, High | 0.0990 | .5938 |
| Close, ArgMax | 0.1037 | .6222 |
| High, Low | 0.09911 | .5947 |
| Argmax, High | 0.11585 | 0.6951 |
| ArgMax, ArgMin | 0.1574 | 0.9444 |
| Close, High, Low | 0.0701 | .4204 |
| Close, High, ArgMax | 0.07535 | .4521 |

Expected time average variance reduction. We multiply the variance by 6 in the third column to compare with knowing only the final value, c .

13 Appendix: Integral Evaluations

13.1 Close and High

We now evaluate the integrals M_m in (3.15)-(3.17). Set $r \equiv 2h - c$, $z_2 = h - \mu_2 = -z_3 = h - (2h - c)t$ and $z_4 = h - \mu_4 = ct - h$. For $m = 1$, (3.16) reduces to

$$M_1 \equiv \sqrt{\frac{2}{\pi}} e^{-\frac{g_4}{2}} \int_{-\infty}^{h-\mu_4} \phi_{\sigma^2} + \sqrt{\frac{2}{\pi}} \sum_{i=2}^3 e^{-\frac{g_i}{2}} \int_{-\infty}^{h-\mu_i} ((2h - c)(x + \mu_i) - \tau_i) \phi_{\sigma^2}(x) dx = \tag{13.1}$$

$$\sum_{i=2}^4 \frac{s_i}{\sqrt{2\pi}} e^{-\frac{g_i}{2}} [\tau_i - r\mu_i(1 - \delta_{i,4})] [1 + \operatorname{erf}\left(\frac{h - \mu_i}{\sqrt{2\sigma}}\right)] - \frac{2\sigma r}{\pi} e^{-\frac{-r^2}{2}} e^{-\frac{(h-rt)^2}{2\sigma^2}} = \tag{13.2}$$

$$\frac{e^{-\frac{c^2}{2}}}{\sqrt{2\pi}} [1 + \operatorname{erf}\left(\frac{ct - h}{\sqrt{2\sigma}}\right)] + \frac{e^{-\frac{r^2}{2}}}{\sqrt{2\pi}} [2hr - 1 + p_{h,r,t} \operatorname{erf}\left(\frac{h - rt}{\sqrt{2\sigma}}\right)] - \frac{2\sigma r}{\pi} * e^{-\frac{-r^2}{2}} e^{-\frac{(h-rt)^2}{2\sigma^2}} \tag{13.3}$$

For the second moment, (3.15) reduces to

$$M_2 \equiv \sqrt{\frac{2}{\pi}} \sum_{i=2}^4 s_i e^{-\frac{g_i}{2}} \int_{-\infty}^{h-\mu_i} [2(x + \mu_i)\tau_i - (2h - c)(x + \mu_i)^2(1 - \delta_{i,4})] \phi_{\sigma^2}(x) dx \tag{13.4}$$

$$= \sqrt{\frac{2}{\pi}} \sum_{i=2}^4 2s_i \tau_i e^{-\frac{g_i}{2}} \left[\frac{\mu_i}{2} [1 + \operatorname{erf}\left(\frac{h - \mu_i}{\sqrt{2\sigma}}\right)] - \sigma^2 \phi_{\sigma^2}(h - \mu_i) \right] \tag{13.5}$$

$$+ (2h - c) \sqrt{\frac{2}{\pi}} \exp^{-\frac{r^2}{2}} \sum_{i=2}^3 \left[\frac{(\mu_i^2 + \sigma^2)}{2} \left[\operatorname{erf}\left(\frac{h - \mu_i}{\sqrt{2\sigma}}\right) + 1 \right] - (h + \mu_i) \sigma^2 \phi_{\sigma^2}(h - \mu_i) \right] \tag{13.6}$$

$$= \sqrt{\frac{2}{\pi}} \sum_{i=2}^4 s_i \mu_i \tau_i e^{-\frac{g_i}{2}} [1 + \operatorname{erf}\left(\frac{h - \mu_i}{\sqrt{2\sigma}}\right)] \tag{13.7}$$

$$- \sqrt{\frac{2r}{\pi}} \exp^{-\frac{r^2}{2}} \left(\left[\sigma^2 + \frac{\mu_2^2 + \mu_3^2}{2} + \frac{\mu_2^2 - \mu_3^2}{2} \operatorname{erf}\left(\frac{z_2}{\sqrt{2\sigma}}\right) \right] - 4h\sigma^2 \phi_{\sigma^2}(z_2) \right) = \tag{13.8}$$

$$\sqrt{\frac{2}{\pi}} [(2h - ct) e^{-\frac{c^2}{2}} [1 + \operatorname{erf}\left(\frac{ct - h}{\sqrt{2\sigma}}\right)] - \sqrt{\frac{2}{\pi}} e^{-\frac{r^2}{2}} [q_3(h, c, t) + q_4(h, c, t) \operatorname{erf}\left(\frac{h - rt}{\sqrt{2\sigma}}\right)]] \tag{13.9}$$

$$+ \sqrt{\frac{2r}{\pi}} \exp^{-\frac{r^2}{2}} \left(\left[\sigma^2 + q_5(h, c, t) + \frac{4h(rt - h)}{2} \operatorname{erf}\left(\frac{h - rt}{\sqrt{2\sigma}}\right) \right] - 4h\sigma^2 \phi_{\sigma^2}(h - rt) \right) \tag{13.10}$$

where we define $q_3(h, c, t) \equiv \mu_2\tau_2 + \mu_3\tau_3 = rt^2 + (1 - t)(2h - rt)$, $q_4(h, c, t) \equiv \mu_2\tau_2 - \mu_3\tau_3 = rt - 2h(1 - t)$, $q_5(h, c, t) \equiv \mu_2^2 + \mu_3^2 = r^2t^2 + (2h - rt)^2$ and $\mu_2^2 - \mu_3^2 = 4h(rt - h)$. For (13.7), we use

$$C_1(H, \mu) \equiv \int_{-\infty}^{H-\mu} (x + \mu) \phi_{\sigma^2}(x) = \frac{\mu}{2} \left[\operatorname{erf}\left(\frac{H - \mu}{\sqrt{2\sigma}}\right) + 1 \right] - \sigma^2 \phi_{\sigma^2}(H - \mu) , \tag{13.11}$$

$$C_2(H, \mu) \equiv \int_{-\infty}^{H-\mu} (x + \mu)^2 \phi_{\sigma^2}(x) = \frac{\mu^2 + \sigma^2}{2} \left[\operatorname{erf}\left(\frac{H - \mu}{\sqrt{2\sigma}}\right) + 1 \right] - \sigma^2 (H + \mu) \phi_{\sigma^2}(H - \mu) . \tag{13.12}$$

These formulas have been verified by numerically integrating the moments of $\partial_h F(x, t, h, c)$ from $-\infty$ to h .

13.2 High, Low, Close

We begin by showing the boundary terms in (8.13) vanish. Here $\mathcal{B}_{ijk}(x = H) = -s_i h^m [(A_{ijk}/\sigma^2) \partial_x f_{ijk}(h) + B_{ijk} f_{ijk}(h)]$. To show these boundary terms vanish, we note $f_{ijk}(h) = f_{1jk}(h)$, $\partial_x f_{ijk}(h) = (\mu_{ijk} - h) f_{1jk}(h)$. Since $\tau_{1jk} \hat{\tau}_{1jk} - \tau_{4jk} \hat{\tau}_{4jk} = -2v_{jk}$, $\tau_{2jk} \hat{\tau}_{2jk} - \tau_{3jk} \hat{\tau}_{3jk} = -2\tilde{v}_{jk}$, we have $\sum_{i=1}^4 s_i A_{ijk} \partial_x f_{ijk}(h) = f_{1jk}(h) \sum_{i=1}^4 s_i A_{ijk} (\mu_{ijk} - h) = 2(\tilde{v}_{jk} * (h - \mu_{4jk}) - v_{jk} * (h - \mu_{3jk}))/\sigma^2$. Expanding μ_{ijk} yields $[\tilde{v}_{jk} * (\mu_{4jk} - h) - v_{jk} * (\mu_{3jk} - h)] = [4jc + 4h(k - j) - 16jk\Delta_{hl}]\sigma^2$. To simplify $\sum_i s_i B_{ijk}$, note $\tau_{1jk} + \tau_{4jk} = 2$, $\tau_{2jk} + \tau_{3jk} = 2$, $\hat{\tau}_{1jk} + \hat{\tau}_{4jk} = 0$ and $\hat{\tau}_{2jk} + \hat{\tau}_{3jk} = 0$. Summing pairs of B_{ijk} yields $B_{1jk} + B_{4jk} = \partial_\ell g_1 [\tau_{1jk} + \tau_{4jk} - \hat{\tau}_{1jk} - \hat{\tau}_{4jk}] = 2\partial_\ell g_1$ and $B_{2jk} + B_{3jk} = \partial_\ell g_2 [\tau_{2jk} + \tau_{3jk} - \hat{\tau}_{2jk} - \hat{\tau}_{3jk}] = 2\partial_\ell g_2$. Finally, $\partial_\ell g_1 - \partial_\ell g_2 = (c - w_{jk} * \Delta_{hl}) * w_{jk} - (2 * h - c - \tilde{w}_{jk} * \Delta_{hl}) * \tilde{w}_{jk} = [8jk\Delta_{hl} + 4jc + 2h(k - j)]$. This shows that $\sum_{i=1}^4 \mathcal{B}_{ijk}(x = h)$ vanishes. For the lower boundary, we regroup the sum using $j \rightarrow \hat{j} = j + 1$, $k \rightarrow \hat{k} = k - 1$. This corresponds to centering the generator relative to ℓ instead of h .

To derive (8.14) and (8.16), we need the following integrals:

$$G_{mn}(\mu, h, \ell) \equiv \int_{\ell - \mu}^{h - \mu} (x + \mu)^m x^n \phi_{\sigma^2}(x) . \quad (13.13)$$

We define the scaled *erf* function, $E_\sigma(x) \equiv .5 * \text{erf}(x/\sqrt{2}\sigma)$ and compute $G_{00}(\mu, h, \ell) = [E_\sigma(h - \mu) - E_\sigma(\ell - \mu)]$ and $G_{01}(\mu, h, \ell) = \sigma^2 [\phi_{\sigma^2}(\ell - \mu) - \phi_{\sigma^2}(h - \mu)]$,

$$G_{10}(\mu, h, \ell) = \mu [E_\sigma(h - \mu) - E_\sigma(\ell - \mu)] + \sigma^2 [\phi_{\sigma^2}(\ell - \mu) - \phi_{\sigma^2}(h - \mu)] \quad (13.14)$$

$$G_{20}(h, \ell) = (\sigma^2 + \mu^2) [E_\sigma(h - \mu) - E_\sigma(\ell - \mu)] + \sigma^2 [(\ell + \mu)\phi_{\sigma^2}(\ell - \mu) - (h + \mu)\phi_{\sigma^2}(h - \mu)] \quad (13.15)$$

$$G_{11}(\mu, h, \ell) = \sigma^2 [E_\sigma(h - \mu) - E_\sigma(\ell - \mu)] + \sigma^2 [\ell\phi_{\sigma^2}(\ell - \mu) - h\phi_{\sigma^2}(h - \mu)] . \quad (13.16)$$

We now simplify (8.16). To simplify the lower limit values at ℓ , we need to define the analog of μ_{ijk} except that the definitions are centered at the lower limit. Let $\nu_{1,j,k} = ct + \tilde{v}_{j,k}\Delta$, $\tilde{g}_1 = (c - w_{j,k}\Delta)^2/2$, $\nu_2 = (2\ell - c)t + v_{j,k}\Delta$, $\tilde{g}_2 = (2\ell - c - \tilde{w}_{j,k}\Delta)^2/2$, $\nu_3 = 2\ell(1 - t) + ct - v_{j,k}\Delta$ and $\nu_4 = 2\ell - ct - \tilde{v}_{j,k}\Delta$. Of course, $\tilde{g}_4 = \tilde{g}_1 = g_1$ and $\tilde{g}_3 = \tilde{g}_2$. The analog of (8.8) is

$$G(x, t, h, \ell, c) = \sum_{j,k > -\infty} \sum_{i=1}^4 \frac{s_i}{\sqrt{2\pi}} \phi_{\sigma^2}(x - \nu_{ijk}) e^{-\tilde{g}_{ijk}(h, \ell)} , \quad (13.17)$$

We further define $\tilde{\tau}_{ijk} \equiv \partial_h \nu_{ijk}$ and $\hat{\tau}_{ijk} \equiv \partial_\ell \nu_{ijk}$. Thus $\tilde{\tau}_{1jk} = \tilde{v}_{j,k} = -\hat{\tau}_{1jk}$, $\tilde{\tau}_{2jk} = v_{j,k}$, $\hat{\tau}_{2jk} = 2t - v_{j,k}$, $\tilde{\tau}_{3jk} = -v_{j,k}$, $\hat{\tau}_{3jk} = 2(1 - t) + v_{j,k}$, $\tilde{\tau}_{4jk} = -\tilde{v}_{j,k}$ and $\hat{\tau}_{4jk} = 2 + \tilde{v}_{j,k}$. Finally, we need $A_{ijk}^\ell = \tilde{\tau}_{ijk} \hat{\tau}_{ijk}$, $B_{ijk}^\ell = [\tilde{\tau}_{ijk} \partial_\ell \tilde{g}_{ijk} + \hat{\tau}_{ijk} \partial_h \tilde{g}_{ijk}]$ and $C_{ijk}^\ell = \tilde{\Gamma}_{ijk} + \sigma^{-2} \tilde{\tau}_{ijk} \hat{\tau}_{ijk}$ and $\tilde{\Gamma}_{ijk} \equiv -\partial_h \tilde{g}_{ijk} \partial_\ell \tilde{g}_{ijk} + \partial_\ell \partial_h \tilde{g}_{ijk}$. Note $\tilde{\Gamma}_{1jk} = \Gamma_{1jk}$ and

We now rewrite (8.16) by summing the Gaussian over i :

$$M_m = \sum_{j,k} U_{jk}^{m,h} f_{1jk}(h - \mu_{1jk}) - U_{jk}^{m,\ell} f_{1jk}(\ell - \mu_{1jk}) + \sum_{ijk} \frac{s_i}{\sqrt{2\pi}} e_{ijk}^{(m)} [W_{ijk}(h - \mu_{ijk}) - W_{ijk}(\ell - \mu_{ijk})] \quad (13.18)$$

where $W_{ijk}(x) \equiv e^{-g_{ijk}} E_\sigma(x)$. The coefficients, $e_{ijk}^{(m)}$ are defined below (8.16). The coefficients satisfy

$$U_{jk}^{1h} = \sum_i s_i A_{ijk} + 2(\Gamma_{2jk} - \Gamma_{1jk})\sigma^2 = \bar{A}_{jk}\sigma^2 + 2(\Gamma_{2jk} - \Gamma_{1jk})\sigma^2 \quad (13.19)$$

where $\bar{A}_{jk} = \sum_i s_i A_{ijk}/\sigma^2 = 32jk + 8(j - k)$. For the lower limit,

$$U_{jk}^{1\ell} = \sum_i s_i A_{ijk}^\ell + 2(\tilde{\Gamma}_{2jk} - \Gamma_{1jk})\sigma^2 = \bar{A}_{jk}^\ell \sigma^2 + 2(\tilde{\Gamma}_{2jk} - \Gamma_{1jk})\sigma^2 \quad (13.20)$$

where $\bar{A}_{jk}^\ell = \sum_i s_i A_{ijk}^\ell/\sigma^2 = 32jk - 8(j - k)$. For the second moment,

$$U_{jk}^{2h} = 2h \sum_i s_i A_{ijk} - 2\sigma^2 \sum_i s_i B_{ijk} + 4h\sigma^2(\Gamma_{2jk} - \Gamma_{1jk}) = 2h\bar{A}_{jk}\sigma^2 + \bar{B}_{jk} + 4h\sigma^2(\Gamma_{2jk} - \Gamma_{1jk}) \quad (13.21)$$

where $\bar{B}_{jk} = 2\partial_\ell(g_1 - g_2) = \sum_i s_i B_{ijk} = 8c * j - 8h(j - k) - 32jk\delta$

$$U_{jk}^{2\ell} = 2\ell \sum_i s_i A_{ijk}^\ell - 2\sigma^2 \sum_i s_i B_{ijk}^\ell + 4\ell\sigma^2(\tilde{\Gamma}_{2jk} - \Gamma_{1jk}) = 2\ell \bar{A}_{jk}^\ell \sigma^2 + \bar{B}_{jk} + 4\ell\sigma^2(\Gamma_{2jk}^\ell - \Gamma_{1jk}) \quad (13.22)$$

where $\bar{\bar{B}}_{jk} = \sum_i s_i B_{ijk}^\ell = 2\partial_h(\tilde{g}_1 - \tilde{g}_2) = 32jk\delta - 8c * j + 8\ell(j - k)$

It is possible to make small additional simplifications of (13.18), but the resulting moment computations are not much simpler than (13.18). The computation remains a two dimensional infinite sum. We content ourselves with only one more identity: $\tilde{\Gamma}_{3jk} = (2\tilde{g}_{2jk} - 1)\tilde{w}_{jk}(\tilde{w}_{jk} + 2) = \tilde{w}_{jk}(\tilde{w}_{j,k} + 2)[(2\ell - c - \tilde{w}_{j,k}\Delta)^2 - 1]$.

References

- [1] T.G. Andersen, T. Bollerslev and J. Cai. Intraday and interday volatility in Japanese stock market. *J. of Int. Financial Markets, Institutions and Money*, 10, 107-130 (2000).
- [2] S. Asmussen, P. Glynn, and J. Pitman. Discretization error in simulation of one-dimensional reflecting Brownian motion. *Ann. Applied Probab.*, 5, pp. 875-896, (1995), MR97e:65156.
- [3] J. Bertoin and J. Pitman, Path transformations connecting Brownian bridge, excursion and meander. *Bull. Sci. Math.* 2(118), pp. 147-166 (1994).
- [4] A.N. Borodin and P. Salminen. *Handbook of Brownian Motion: Facts and Formulae*. Birkh user, Basel (2002) MR-1477407.
- [5] B. Choi and J. Roh. On the trivariate joint distribution of Brownian motion and its maximum and minimum. *Statistics and Probability Letters*, Volume 83, (2013), pp. 1046-1053.
- [6] Luc Devroye. On exact simulation algorithms for some distributions related to Brownian motion and Brownian meanders. *Recent developments in Applied Probability and Statistics*, pp. 1-35, 2010 -Physica-Verlag HD.
- [7] R. T. Durrett, D. L. Iglehart, and D. R. Miller, Weak convergence to Brownian meander and Brownian excursion, *Ann. Probability*, 5, (1977), pp. 117-129, MR-55:9300.
- [8] R. T. Durrett and D. L. Iglehart. Functionals of Brownian Meander and Brownian Excursion. *The Annals of Probability* Vol. 5, No. 1 (Feb., 1977), pp. 130-135.
- [9] H. Fayed and A. Atiya, An evaluation of the integral of the product of the error function and the normal probability density with application to the bivariate normal integral. *Mathematics of Computation*, 83, (2014), pp. 235-250.
- [10] W. Feller. The asymptotic distribution of the range of sums of independent random variables. *Ann. Math. Statistics*, 22 :427-432, (1951) MR-042626.
- [11] M. Garman and M. Klass. On the Estimation of Security Price Volatilities from Historical Data. *Journal of Business*. 53, pp.67-78. 1980.
- [12] J. P. Imhof. Density factorizations for Brownian motion, meander and the three-dimensional Bessel process, and applications. *J. Appl. Probab.*, 21:500-510, 1984. Math. Review MR-85j:60152.
- [13] J. P. Imhof. On Brownian bridge and excursion *Studia Sci. Math. Hungar.*, 20:1-10, 1985. Math. Review MR-88h:60159.
- [14] I. Karatzas and S. E. Shreve, *Brownian Motion and Stochastic Calculus*. Second Edition, Springer, New York, 1998, MR1121940.
- [15] Paul L vy. *Processus Stochastiques et Mouvement Brownien*. Gauthier-Villars, Paris, 1948 MR-0190953.
- [16] D.L. McLeish. Highs and lows: Some properties of the extremes of a diffusion and applications in finance. *Canadian Journal of Statistics*, 30, pp.243-267, 2002.
- [17] I. Meilijson. The Garman-Klass Estimator revisited. *REVSTAT Statistical Journal*, Vol. 9 pp. 199-212 (2011).
- [18] Gregory L. Morris. *Candlestick Charting Explained*. McGraw-Hill, Third Edition (2006).
- [19] K.S. Riedel. A gallery of the mean and variance of Brownian motion with given final value, maximum and argmax. submitted.
- [20] L.C.G. Rogers and S.E. Satchell. Estimating variance from high, low, closing prices. *Ann. Applied Probability* 1 504-512, 1991.
- [21] L. A. Shepp. The joint density of the maximum and its location for a Wiener process with drift. *Journal of Applied Probability*, vol. 16, pp. 423-427, 1979.
- [22] D. Williams. Decomposing the Brownian path. *Bull. Amer. Math. Soc.*, 76:871-873, 1970. Math. Review MR-41.